Stereochemistry Modulates the Stability of Reduced Interstrand Cross-Links Arising from *R*- and *S*-α-CH_3-γ-OH-1,N^2-Propano-2′-deoxyguanosine in the 5′-CpG-3′ DNA Sequence†

Young-Jin Cho, Ivan D. Kozekov, Thomas M. Harris, Carmelo J. Rizzo, and Michael P. Stone*

Department of Chemistry, Center in Molecular Toxicology, Vanderbilt-Ingram Cancer Center, Vanderbilt University, Nashville, Tennessee 37235

Received July 7, 2006; Revised Manuscript Received December 13, 2006

ABSTRACT: The solution structures of 5′-Cp-N^2-dG-3′-*R*-(α)-CH_3-propyl-5′-Cp-N^2-dG-3′ and 5′-Cp-N^2-dG-3′-*S*-(α)-CH_3-propyl-5′-Cp-N^2-dG-3′ interstrand DNA cross-links in the 5′-CpG-3′ sequence were determined by NMR spectroscopy. These were utilized as chemically stable surrogates for the corresponding carbinolamine interstrand cross-links arising from the crotonaldehyde- and acetaldehyde-derived *R*- and *S*-α-CH_3-γ-OH-1,N^2-propanodeoxyguanosine adducts. The results provide an explanation for the observation that interstrand cross-link formation in the 5′-CpG-3′ sequence by the *R*- and *S*-α-CH_3-γ-OH-1,N^2-propanodeoxyguanosine adducts is dependent upon stereochemistry, favoring the *R*-α-CH_3-γ-OH-1,N^2-propanodeoxyguanosine adduct [Kozekov, I. D., Nechev, L. V., Moseley, M. S., Harris, C. M., Rizzo, C. J., Stone, M. P., and Harris, T. M. (2003) *J. Am. Chem. Soc. 125*, 50−61]. Molecular dynamics calculations, restrained by NOE-based distances and empirical restraints, revealed that both the 5′-Cp-N^2-dG-3′-*R*-(α)-CH_3-propyl-5′-Cp-N^2-dG-3′ and 5′-Cp-N^2-dG-3′-*S*-(α)-CH_3-propyl-5′-Cp-N^2-dG-3′ cross-links were located in the minor groove and retained Watson−Crick hydrogen bonds at the tandem cross-linked C·G base pairs. However, for the 5′-Cp-N^2-dG-3′-*R*-(α)-CH_3-propyl-5′-Cp-N^2-dG-3′ cross-link, the (α)-CH_3 group was positioned in the center of the minor groove, whereas for the 5′-Cp-N^2-dG-3′-*S*-(α)-CH_3-propyl-5′-Cp-N^2-dG-3′ cross-link, the (α)-CH_3 group was positioned in the 3′ direction, showing steric interference with the DNA helix. The 5′-Cp-N^2-dG-3′-*S*-(α)-CH_3-propyl-5′-Cp-N^2-dG-3′ cross-link exhibited a lower thermal stability as evidenced by NMR spectroscopy as a function of temperature. The two cross-links also exhibited apparent differences in the conformation of the interstrand three-carbon cross-link, which may also contribute to the lower apparent thermodynamic stability of the 5′-Cp-N^2-dG-3′-*S*-(α)-CH_3-propyl-5′-Cp-N^2-dG-3′ cross-link.

Crotonaldehyde **1**, an α,β-unsaturated aldehyde, is genotoxic and mutagenic in human lymphoblasts (*1*). It induces liver tumors in rodents (*2*). Michael addition of deoxyguanosine to crotonaldehyde yields the diastereomeric *R*- and *S*-α-CH_3-γ-OH-1,N^2-propano-2′-deoxyguanosine adducts **2a** and **2b**, respectively (Chart 1) (*3*−*6*). A second DNA adduction pathway yields paraldol-releasing DNA adducts (*7*), primarily N^2-(3-hydroxybutylidene)-dG (*8*). Adducts **2a** and **2b** also form through the reaction of acetaldehyde, a mutagen and potential human carcinogen (*9*), with deoxyguanosine (*6*, *10*). The *R*- and *S*-α-CH_3-γ-OH-PdG adducts **2a** and **2b** have been detected in human and rodent tissues (*11*−*13*). In humans, these probably result from various endogenous and exogenous exposures, including lipid peroxidation (*11*, *14*, *15*), exposure to tobacco smoke (*16*, *17*), and exposure to *N*-nitrosopyrrolidine (*18*, *19*).

The site-specific synthesis of oligodeoxynucleotides containing cyclic adduct **2a** or **2b** (*20*−*22*) enabled their chemistry to be examined in duplex DNA. When adduct **2a** or **2b** was placed into oligodeoxynucleotide duplexes at 5′-CpG-3′ sequences, Kozekov et al. (*23*) trapped interstrand saturated three-carbon cross-links by treatment with $Na(CN)BH_3$, corroborating the reports of Wang et al. (*6*, *8*). Significantly, cross-linking efficiency was dependent upon the stereochemistry of the adduct, favoring *R*-α-CH_3-γ-OH-PdG adduct **2a**, as opposed to *S*-α-CH_3-γ-OH-PdG adduct **2b**. However, both *R*-α-CH_3-γ-OH-PdG adduct **2a** and *S*-α-CH_3-γ-OH-PdG adduct **2b** readily formed N-terminal conjugates with the peptide KWKK (*24*). This implied that both adducts **2a** and **2b** underwent opening to the corresponding aldehydes **3a** and **3b**, respectively, when placed opposite dC in duplex DNA, but only aldehyde **3a** efficiently formed interstrand cross-links in the 5′-CpG-3′ sequence.

A series of stable isotope-edited NMR experiments showed that crotonaldehyde-derived adduct **2a** yielded carbinolamine cross-link **5a**, with the corresponding imine **6a** and pyrimidopurinone **7a** cross-links remaining below the level of detection at equilibrium in duplex DNA (*25*). Molecular modeling suggested a thermodynamic basis for this observa-

† This work was supported by NIH Grant ES-05335 (T.M.H., C.J.R., and M.P.S.). Funding for the NMR spectrometers was supplied by Vanderbilt University, by NIH Grant RR-05805, and the Vanderbilt Center in Molecular Toxicology, Grant ES-00267. The Vanderbilt-Ingram Cancer Center is supported by NIH Grant CA-68485.

* To whom correspondence should be addressed. Telephone: (615) 322-2589. Fax: (615) 322-7591. E-mail: michael.p.stone@vanderbilt.edu.

10.1021/bi061381h CCC: $37.00
Published on Web 02/17/2007

Chart 1: Equilibrium Chemistry of the *R*- and *S*-α-CH_3-γ-OH-PdG Adducts in the 5′-CpG-3′ Sequence in Duplex DNA

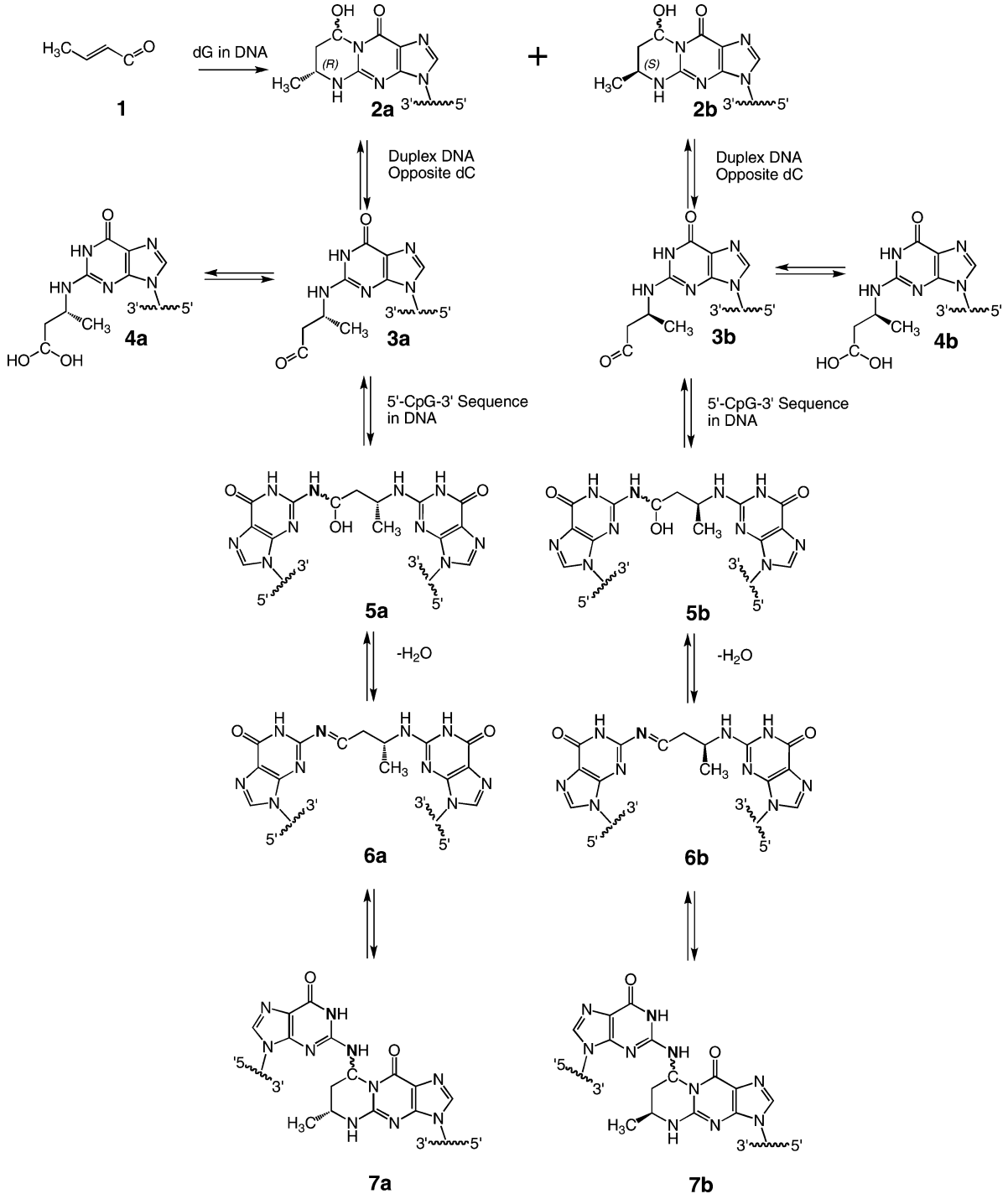

tion: the interstrand cross-link arising from the N^2-(*R*-α-CH_3-γ-OH-1,N^2-propano-2′)-dG adduct **2a** introduced less disruption into the duplex than did that arising from the N^2-(*S*-α-CH_3-γ-OH-1,N^2-propano-2′)-dG adduct **2b**, due to differing orientations of the *R*- and *S*-CH_3 groups (*25*).

Herein, solution structures of stereoisomeric reduced 5′-Cp-N^2-dG-3′-*R*-(α)-CH_3-propyl-5′-Cp-N^2-dG-3′ and 5′-Cp-N^2-dG-3′-*S*-(α)-CH_3-propyl-5′-Cp-N^2-dG-3′ interstrand DNA cross-links **8a** and **8b** in the 5′-CpG-3′ sequence (Chart 2) are determined by NMR spectroscopy. These are utilized as chemically stable surrogates for the carbinolamine interstrand cross-links **5a** and **5b** arising from the crotonaldehyde- and acetaldehyde-derived *R*- and *S*-α-CH_3-γ-OH-1,N^2-propanodeoxyguanosine adducts. A similar strategy was employed by Liu et al. (*26*) to examine replication-coupled repair of these crotonaldehyde- and acetaldehyde-derived interstrand cross-links. These structural data explain the observation that interstrand cross-link formation in the 5′-CpG-3′ sequence favors N^2-(*R*-α-CH_3-γ-OH-1,N^2-propano-2′)-dG adduct **2a** (*23*). Molecular dynamics calculations, restrained by NOE-based distances and empirical restraints, reveal that both cross-links **8a** and **8b** are located in the minor groove and retain Watson−Crick hydrogen bonds at the tandem cross-linked C·G base pairs. However, for cross-link **8a**, the (α)-CH_3 group is positioned in the center of the minor groove, whereas for cross-link **8b**, the (α)-CH_3 group interferes

Chart 2: (A) Duplex Oligodeoxynucleotide Containing the 5′-CpG-3′ Sequence, (B) Reduced *R*-α-CH_3-γ-OH-1,N^2-Propano-2′-deoxyguanosine Cross-Linked Adduct **8a**, and (C) Reduced *S*-α-CH_3-γ-OH-1,N^2-Propano-2′-deoxyguanosine Cross-Linked Adduct **8b**

A

5′-G^1 C^2 T^3 A^4 G^5 C^6 **X^7** A^8 G^9 $T^{10}C^{11}C^{12}$-3′
3′-$C^{24}G^{23}A^{22}T^{21}C^{20}$**$Y^{19}$**$C^{18}T^{17}C^{16}A^{15}G^{14}G^{13}$-5′

B

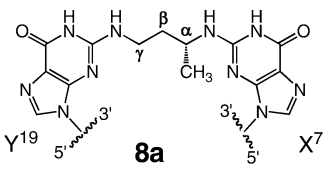

8a

C

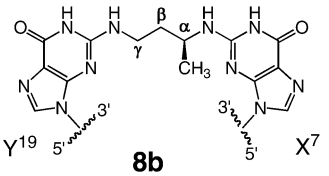

8b

sterically with the DNA helix. Cross-link **8b** exhibits a lower thermal stability as evidenced by NMR spectroscopy as a function of temperature. The two cross-links also exhibit differences in the conformation of the interstrand three-carbon cross-link, which may contribute to the lower thermodynamic stability of cross-link **8b**.

MATERIALS AND METHODS

Oligodeoxynucleotide Synthesis. Oligodeoxynucleotides containing site-specific α-CH_3-γ-OH-PdG adducts were prepared as previously described (*20*−*22*). All commercially obtained chemicals were used as received. Concentrations of the single-stranded oligodeoxynucleotides were determined from calculated extinction coefficients at 260 nm (*27*). The concentrations of the single-stranded oligodeoxynucleotides were determined from extinction coefficients of 11.3 × 10^4 and 11.1 × 10^4 cm^{-1}, respectively, at 260 nm.

HPLC. Oligodeoxynucleotide purification and analysis of enzymatic digestions were performed on a Beckman HPLC system (32 Karat software, version 3.1; pump module 125) with a diode array UV detector (module 168) monitoring at 260 nm using a Waters YMC ODS-AQ column [250 mm × 4.6 mm (inside diameter), 1.5 mL/min for analysis, and 250 mm × 10 mm (inside diameter), 5 mL/min for purification]. The mobile phase was CH_3CN in 0.1 M ammonium formate (pH 7.0). Gradient 1 was a linear gradient from 1 to 10% CH_3CN over 15 min, a linear gradient from 10 to 20% CH_3CN over 5 min, 20% isocratic for 5 min, a linear gradient from 20 to 100% CH_3CN over 3 min, 100% isocratic for 2 min, and a linear gradient from 100 to 1% CH_3CN over 3 min. Gradient 2 was a linear gradient from 1 to 5% CH_3CN over 5 min, a linear gradient from 5 to 9.5% CH_3CN over 15 min, a linear gradient from 9.5 to 100% CH_3CN over 3 min, 100% isocratic for 2 min, and a linear gradient from 100 to 1% CH_3CN over 3 min.

Capillary Gel Electrophoresis. Electrophoretic analyses were carried out using a Beckman P/ACE MDQ instrument system (32 Karat software, version 5.0) monitored at 260 nm on a 31.2 cm × 100 μm eCAP capillary with samples applied at 10 kV and run at 9 kV. The capillary was packed with the manufacturer's 100-R gel (for ss-DNA) using a Tris-borate buffer system containing 7 M urea.

Mass Spectrometry. MALDI-TOF[1] mass spectra (negative ion) of modified oligodeoxynucleotides were obtained on a Voyager Elite DE instrument (Perseptive Biosystems) at the Vanderbilt Mass Spectrometry Facility using a 3-hydroxypicolinic acid matrix containing ammonium hydrogen citrate (7 mg/mL) to suppress multiple sodium and potassium adducts.

Enzymatic Digestions. Enzymatic digestion was carried out in one step. The oligodeoxynucleotides (0.2−0.5 A_{260} units) were dissolved in 30 μL of buffer containing 10 mM Tris-HCl and 10 mM $MgCl_2$ (pH 7.0) and incubated with DNase I (8 units; Promega), snake venom phosphodiesterase I (0.02 unit; Sigma), and alkaline phosphatase (1.7 units, *Escherichia coli*; Sigma) at 37 °C for 90 min. The mixture was analyzed by reversed phase HPLC as described above. Adducted deoxynucleosides were identified by comparison with authentic samples on the basis of retention times, co-injection, and UV spectra.

Melting Studies. Cross-linked duplex (0.5 A_{260} unit) was dissolved in 0.5 mL of buffer containing10 mM Na_2HPO_4/NaH_2PO_4, 0.1 M NaCl, and 50 μM Na_2EDTA (pH 7.0). The UV absorbance at 260 nm was monitored at 1 min intervals with a 1 °C/min temperature gradient. The temperature was cycled between 5 and 95 °C. The first derivative of the melting curve was used to establish the T_m values.

N^2-(S-3-Aminobutyl)-2′-deoxyguanosine and N^2-(S-3-Amino-1-methylpropyl)-2′-deoxyguanosine. (*S*)-1,3-Diaminobutane dihydrochloride (30 mg, 0.187 mmol) (*28*) was added to a solution of O^6-(2-trimethylsilylethyl)-2-fluoro-2′-deoxyinosine (10 mg, 0.027 mmol), DMSO (200 μL), and diisopropylethylamine (100 μL). The mixture was stirred at 65 °C for 24 h. The volatiles were removed in vacuo with a centrifugal evaporator. The residue was dissolved in 5% acetic acid (500 μL) and stirred for 2 h at room temperature to remove the O^6-protecting group. The mixture was neutralized with 1 M NaOH and purified by HPLC (gradient 1) to give an 85% combined yield of products. N^2-(*S*-3-Aminobutyl)-2′-deoxyguanosine (7.1 mg): ^{1}H NMR (DMSO-d_6) δ 7.88 (s, 1H, H8), 6.15 (t, J = 7.0 Hz, 1H, H1′), 4.36 (m, 1H, H3′), 3.80 (m, 1H, H4′), 3.56 (m, 1H, H5′), 3.49 (m, 1H, H5″), 3.34 (m, 2H, NH-CH_2), 3.12 (m, 1H, CH-NH_2), 2.60 (m, 1H, H2′), 2.20 (m, 1H, H2″), 1.73 (m, 1H, CH_2-CH), 1.65 (m, 1H, CH_2-CH), 1.15 (d, J = 7.0 Hz, 3H, CH_3), N1H and OH signals not observed. N^2-(*S*-3-Amino-1-methylpropyl)-2′-deoxyguanosine (acetate salt, 0.60 mg): ^{1}NMR (DMSO-d_6) δ 7.87 (s, 1H, H8), 6.13 (dd, 1H, H1′, J_1 = J_2 = 6.4 Hz), 4.35 (m, 1H, H3′), 4.00 (m, 1H, CH-CH_3),

[1] Abbreviations: DQF-COSY, double-quantum-filtered correlation spectroscopy; HMBC, heteronuclear multiple-bond correlation spectroscopy; MALDI-TOF, matrix-assisted laser desorption ionization time-of-flight mass spectrometry; NOE, nuclear Overhauser enhancement; NOESY, nuclear Overhauser enhancement spectroscopy; R_1^x, sixth-root residual; rMD, restrained molecular dynamics; rmsd, root-mean-square deviation; TOCSY, total correlation spectroscopy; TPPI, time-proportional phase increment.

3.80 (m, 1H, H4′), 3.55 (dd, 1H, H5′, $J_1 = 5.2$ Hz, $J_2 = 11.5$ Hz), 3.48 (dd, 1H, H5″, $J_1 = 5.2$ Hz, $J_2 = 11.7$ Hz), 2.65 (m, 2H, CH_2-NH_2), 2.60 (m, 1H, H2′), 2.20 (m, 1H, H2″), 1.80 (s, 3H, CH_3COO), 1.60 (q, 2H, CH-CH_2, $J = 6.9$ Hz), 1.15 (d, 3H, CH_3, $J = 6.1$ Hz), N^1H and OH signals not observed.

N^2-(R or S)-3-Amino-1-methylpropyl-dG-Adducted Oligodeoxynucleotide. Oligodeoxynucleotides (120 A_{260} units) containing (6*S* or 6*R*)-8-hydroxy-6-methyl-5,6,7,8-tetrahydropyrimido[1,2-*a*]purin-10(3*H*)-one (*21*) in 100 μL of potassium phosphate buffer (pH 7.0) and 100 μL of ammonium hydroxide were incubated at room temperature for 24 h and then treated with $NaBH_4$ (1.0 mg, 27.5 μmol) and stirred at room temperature for an additional 2 h. The reactions were quenched with 5% acetic acid (500 μL) and the products isolated by HPLC. For the N^2-(*R*)-3-amino-1-methylpropyl-dG-adducted oligodeoxynucleotide, 66 A_{260} units were purified by HPLC (gradient 1): MALDI-TOF mass spectral analysis, calcd for $[M - H]^-$ 3715.7, found 3715.6. For the N^2-(*S*)-3-amino-1-methylpropyl-dG-adducted oligodeoxynucleotide, 72 A_{260} units were purified: MALDI-TOF mass spectral analysis, calcd for $[M - H]^-$ 3715.7, found 3715.5.

Synthesis of Cross-Linked Oligodeoxynucleotide Duplexes. The N^2-(*R* or *S*)-3-amino-1-methylpropyl-dG-adducted oligodeoxynucleotide and its complement containing O^6-(2-trimethylsilylethyl)-2-fluoro-2′-deoxyinosine were mixed in a plastic test tube with 300 μL of 0.05 M sodium borate buffer (pH 9). The mixture was stirred at 45−47 °C, and the reaction was monitored by HPLC and CGE. The reaction times were 2 days for the *R*-isomer and 5 days for the *S*-isomer. After the reaction was complete, 5% acetic acid (500 μL) was added and the mixture was stirred for 1 h at room temperature. The cross-linked oligodeoxynucleotides were purified by HPLC and desalted on Sephadex G-25. For 5′-Cp-N^2-dG-3′-*R*-(α)-CH_3-propyl-5′-Cp-N^2-dG-3′ cross-link **8a**, 62 A_{260} units were purified by HPLC: MALDI-TOF mass spectrometry, calcd for $[M - H]^-$ 7346.6, found 7349.4. For 5′-Cp-N^2-dG-3′-*S*-(α)-CH_3-propyl-5′-Cp-N^2-dG-3′ cross-link **8b**, 52 A_{260} units were purified by HPLC (gradient 2): MALDI-TOF mass spectrometry, calcd for $[M - H]^-$ 7346.6, found 7345.1.

NMR. Experiments were carried out at ^{1}H frequencies of 500.13, 600.13, and 800.19 MHz. The duplex oligodeoxynucleotides were prepared at a concentration of 2 mM in 0.25 mL of 99.996% D_2O. The samples contained 10 mM NaH_2PO_4, 0.1 M NaCl, and 50 μM Na_2EDTA (pH 7.0). The samples were placed into micro-NMR tubes (Shigemi Glass, Inc., Allison Park, PA). ^{1}H NOESY experiments in D_2O were conducted at 30 °C. For each t_1 increment, 32 scans were averaged with presaturation of the HDO resonance. To derive distance restraints, spectra were recorded consecutively using TPPI phase cycling with mixing times of 60, 150, 250, and 350 ms. These were recorded with 2048 complex points in the acquisition dimension and 1024 real data points in the indirect dimension covering 9615.385 Hz. The relaxation delay was 2 s. The data in the d_2 dimension were zero-filled to give a matrix of 2K × 2K real points. NOESY spectra for observation of exchangeable protons were recorded at 13 °C, in a 9:1 H_2O/D_2O mixture, using a field gradient Watergate pulse sequence (*29*) for water suppression. The spectra, consisting of 128 transients, were obtained with a cryogenic probe using States−TPPI phase cycling with mixing times of 200 and 250 ms. A squared sine bell with a 72° shift apodization was applied in the d_1 dimension, while cosine-squared bell apodization was applied in the d_2 dimension. A total of 1536 real data points in the d_1 dimension and 512 points in the d_2 dimension were acquired. Double-quantum-filtered ^{1}H correlation (DQF-COSY) spectra (*30*, *31*) were collected at 30 °C with 2048 complex points in the acquisition dimension and 512 points in the d_2 dimension covering 6009.615 Hz and zero-filled to 1024 points to give a matrix of 1024 × 2048 real points. For each d_1 increment, 64 or 84 transients were averaged with presaturation of the HDO resonance. A squared sine-bell apodization function was applied in both dimensions. Chemical shifts of proton resonances were referenced to water. NMR data were processed on Silicon Graphics Octane workstations using NMRPipe (*32*) and assigned using FELIX2000 (Accelrys, Inc., San Diego, CA).

Experimental Distance Restraints. Footprints were drawn around cross-peaks for the NOESY spectrum measured at a mixing time of 250 ms to define the size and shape of individual cross-peaks, using FELIX2000. Identical footprints were transferred and fit to the cross-peaks obtained at the other two mixing times. Cross-peak intensities were determined by volume integration of the areas under the footprints. The intensities were combined with intensities generated from complete relaxation matrix analysis of a starting DNA structure to generate a hybrid intensity matrix (*33*). MARDIGRAS (version 5.2) (*34*, *35*) was used to refine the hybrid matrix by iteration to optimize the agreement between the calculated and experimental NOE intensities. The molecular motion was assumed to be isotropic. The noise level was set at the intensity of the weakest cross-peak. Calculations were performed using the DNA starting models generated using INSIGHT II (Accelrys, Inc.), and NOE intensities were derived from experiments at three mixing times, and with three τ_c values (2, 3, and 4 ns), yielding 18 sets of distances. Analysis of these data yielded the experimental distance restraints and standard deviations for the distance restraints used in subsequent restrained molecular dynamics calculations. For partially overlapped cross-peaks, the upper bounds on the distances were increased.

Restrained Molecular Dynamics. Calculations were performed on Silicon Graphics Octane workstations using AMBER 8.0 (*36*). Classical A-DNA and B-DNA structures were used as reference structures to create starting structures for potential energy minimization (*37*). The reduced cross-links were constructed between X^7 and Y^{19} using the BUILDER module of INSIGHT II (Accelrys, Inc.). ANTECHAMBER was used, and the atom types were based on AMBER atom types for parametrization. RESP atomic charges were calculated using GAUSSIAN98 (*38*) and the Hartree−Fock 6-31G* basis set. Initially constructed A- and B-DNA starting structures were energy-minimized by the conjugate gradient method for 250 iterations using the AMBER 8.0 force field to relieve poor van der Walls contacts. This energy minimization used a constant dielectric without experimental restraints. The restraint energy function included terms describing distance restraints as square-well potentials. The generalized Born solvent model was used for rMD simulated annealing calculations with a salt concentration of 0.1 M, and the SHAKE algorithm was used (*39*, *40*).

The van der Waals energy term used the Lennard-Jones potential energy function. The electrostatic term used the Coulomb function, based on a full set of partial charges (−1 per residue) and a distance-dependent dielectric constant of 4*r*. The nonbonded pair list was updated if any atom moved more than 0.5 Å, and the cutoff radius for nonbonded interactions was 15 Å. The effective energy function included terms describing distance restraints, in the form of square-well potentials. The partial charges assigned to the adduct by RESP protocol are shown in Figure S2 of the Supporting Information.

Calculations were initiated by coupling to a heating bath, with a target temperature of 600 K. The force constants were 50 kcal mol^{-1} Å^{-2} for empirical hydrogen bonding and class 1 NOE restraints and 45, 40, 35, and 30 kcal mol^{-1} Å^{-2} for classes 2−5, respectively. Those force constants were increased 1.5 times during the first 3 ps of heating and reduced to the original values during the rest of the calculations. The target temperature was reached and maintained for 5 ps. The molecules were cooled to 100 K over 12 ps for equilibrium dynamics. During the final 8 ps, the temperature was reduced to 0 K. Coordinate sets were archived every 0.2 ps, and 10 structures from the last 5 ps were averaged in total. An average structure was subjected to 500 iterations of conjugate gradient energy minimization to obtain the final structure. Back-calculation of theoretical NMR intensities from the emergent structures was performed using CORMA (version 5.2) (*33*). Helicoidal parameters were examined using 3DNA (*41*).

RESULTS

*Synthesis of Interstrand Cross-Links **8a** and **8b** Arising from R- and S-α-CH$_3$-γ-OH-1,N^2-Propano-2′-deoxyguanosine Adducts in the 5′-CpG-3′ DNA Sequence.* Dooley et al. (*42*) synthesized trimethylene interstrand cross-links of the type N^2-dG-(CH$_2$)$_3$-N^2-dG using a postoligomerization approach (Scheme 1). This involved the incorporation of O^6-protected 2-fluorohypoxanthine into an oligodeoxynucleotide and its complement at the desired sites for cross-link formation. 1,3-Diaminopropane was reacted with one of the oligodeoxynucleotides, giving the N^2-(3-aminopropyl)-dG-adducted oligodeoxynucleotide. After purification, this oligodeoxynucleotide was reacted with its complementary strand containing an O^6-protected 2-fluorohypoxanthine to give the cross-linked oligodeoxynucleotide. To prepare the reduced crotonaldehyde cross-links using this strategy, (*R*)- and (*S*)-1,3-diaminobutane were required (*28*). This diamine is unsymmetrical; thus, it was critical that the initial adduction reaction with the diamine proceed with high regioselectivity. Lao and Hecht (*10*) reported the application of this strategy. We found that the nucleophilic aromatic substitution reaction of (*R*)-1,3-diaminobutane with excess *O*^{6}-(2-trimethylsilylethyl)-2-fluoroinosine nucleoside gave a 92:8 regiochemical mixture of products (Scheme 1). Consequently, an alternative strategy that would not give such a product mixture was pursued, starting with the stereochemically pure oligodeoxynucleotides containing crotonaldehyde adducts **2a** and **2b** (Scheme 2) (*25*). Reductive amination with ammonia and NaBH$_4$ gave the desired N^2-[3-amino-(1*R*)-methylpropyl]-adducted oligodeoxynucleotides. Condensation with a complementary oligodeoxynucleotide containing 2-fluorohypoxanthine gave the stereo- and regiochemically pure cross-linked

Scheme 1: (A) Synthesis of Trimethylene Interstrand Cross-Links of the Type N^2-dG-(CH$_2$)$_3$-N^2-dG (*42*) and (B) Nucleophilic Aromatic Substitution Reaction of (*S*)-1,3-Diaminobutane with Excess *O*^{6}-(2-Trimethylsilylethyl)-2-fluoroinosine Nucleoside

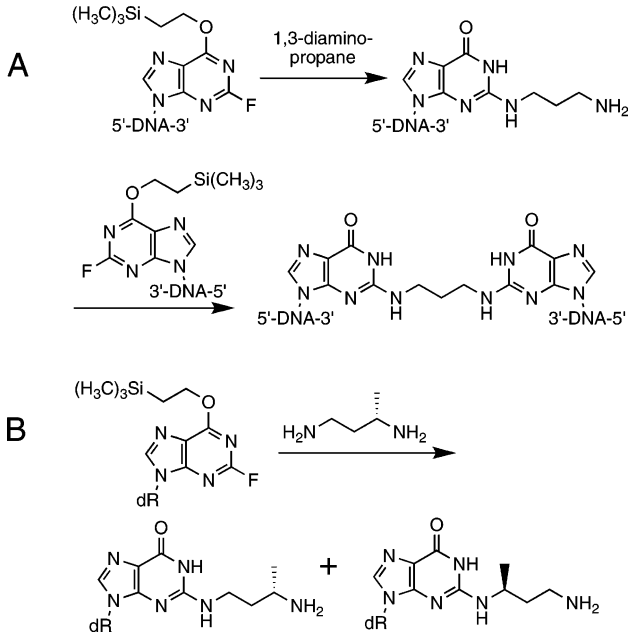

Scheme 2: Synthesis of (A) 5′-Cp-N^2-dG-3′-*R*-(α)-CH$_3$-Propyl-5′-Cp-N^2-dG-3′ and (B) 5′-Cp-N^2-dG-3′-*S*-(α)-CH$_3$-Propyl-5′-Cp-N^2-dG-3′ Interstrand DNA Cross-Links **8a** and **8b**, Respectively, in the 5′-CpG-3′ Sequence

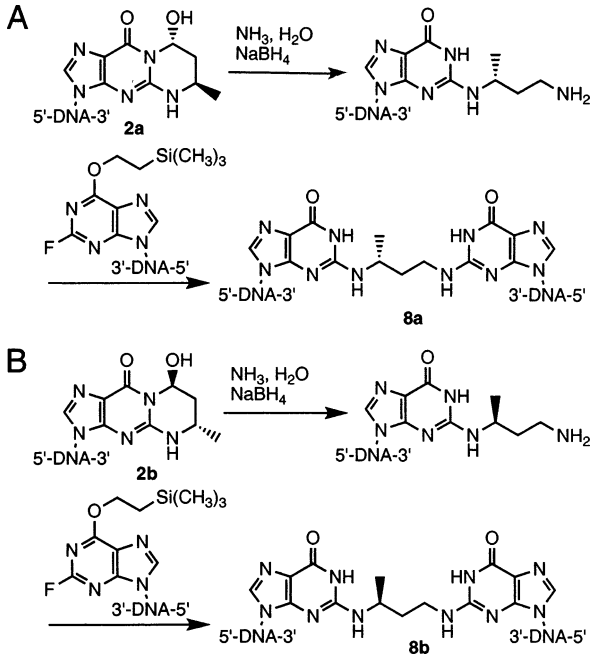

oligodeoxynucleotides **8a** and **8b**, which were characterized by mass spectrometry and enzymatic digestion.

*Thermal Stability of Interstrand Cross-Links **8a** and **8b** Arising from R- and S-α-CH$_3$-γ-OH-1,N^2-Propano-2′-deoxyguanosine Adducts in the 5′-CpG-3′ Sequence.* UV melting studies revealed that the oligodeoxynucleotide containing cross-link **8a** exhibited a T_m higher than that of the oligodeoxynucleotide containing cross-link **8b**. Figure 1 shows the imino proton region of the NMR spectra for the two

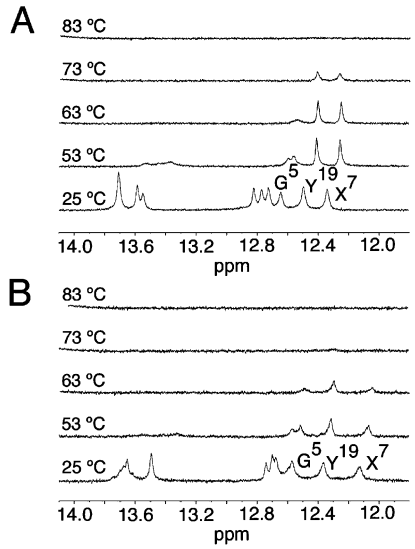

FIGURE 1: Expanded plots showing the imino proton region of the ^{1}H NMR spectrum as a function of temperature. (A) *R*-α-CH_3-γ-OH-1,N^2-Propano-2′-deoxyguanosine cross-linked adduct. (B) *S*-α-CH_3-γ-OH-1,N^2-Propano-2′-deoxyguanosine cross-linked adduct. The data were acquired at a ^{1}H frequency of 500 MHz.

oligodeoxynucleotides containing cross-links **8a** and **8b**, respectively, in the 5′-CpG-3′ sequence, as a function of temperature. For both oligodeoxynucleotides, the N3 imino resonances for T^3, T^{10}, T^{17}, and T^{21} broadened and disappeared at temperatures above 50 °C, whereas the N1 imino resonances for X^7 and Y^{19} were observed at higher temperatures, consistent with the location of the cross-link among these bases. For cross-link **8a** with *R*-stereochemistry, the X^7 and Y^{19} imino resonances remained observable at 73 °C (Figure 1A). In contrast, for cross-link **8b** with *S*-stereochemistry, the X^7 and Y^{19} imino proton resonances broadened and disappeared at this temperature (Figure 1B).

Assignments of Nonexchangeable DNA Protons. (a) 5′-Cp-N^2-dG-3′-R-(α)-CH_3-Propyl-5′-Cp-N^2-dG-3′ Cross-Linked Adduct ***8a***. As shown in panels A and B of Figure 2, the complete sequential connectivity between the aromatic and anomeric protons for both strands was accomplished (*43*, *44*). An overlap occurred for the C^6 and X^7 H1′ resonances. The completion of the NOESY walk was indicative of a stable and ordered DNA conformation. These assignments were expanded into other regions of the spectrum to yield complete ^{1}H assignments for the H2′, H2″, H3′, and H4′ protons. The assignments of Y^{19} H2′ and H2″ were reversed compared to those of other deoxyriboses. Table S1 of the Supporting Information details the assignments of the nonexchangeable protons.

(b) 5′-Cp-N^2-dG-3′-S-(α)-CH_3-Propyl-5′-Cp-N^2-dG-3′ Cross-Linked Adduct ***8b***. As shown in panels C and D of Figure 2, the complete sequential connectivity between the aromatic and the anomeric protons for both strands was accomplished (*43*, *44*). The chemical shifts for X^7 H1′, A^8 H1′, C^{18} H1′, and Y^{19} H1′ differed from those observed in the cross-link having *R*-(α)-CH_3 stereochemistry. Separate resonances were observed for C^6 H1′ at 5.49 ppm and X^7 H1′ at 5.78 ppm. The completion of NOESY walk was indicative of a stable and ordered DNA conformation. These assignments were expanded into other regions of the ^{1}H NOESY spectrum to yield complete ^{1}H assignments for the H2′, H2″, H3′, and H4′ protons. The assignments of Y^{19} H2′ and H2″ were reversed as compared to other deoxyriboses. Table S1 of the Supporting Information details the assignments of the nonexchangeable protons.

Assignments of Exchangeable DNA Protons. (a) 5′-Cp-N^2-dG-3′-R-(α)-CH_3-Propyl-5′-Cp-N^2-dG-3′ Cross-Linked Adduct ***8a***. Figure 3A shows the resonances arising from the Watson−Crick hydrogen-bonded imino protons. The complete sequential NOE connectivity was observed between imino protons except at the terminal bases. The latter resonances were not observed due to rapid exchange with solvent. The imino resonance arising from the C^6•Y^{19} base pair was assigned at 12.6 ppm; the X^7•C^{18} base pair was assigned at 12.5 ppm. Each imino proton exhibited a strong NOE to an amino proton and that of the opposite cytosine. Further, four strong A•T base parings were present, as evidenced by NOEs between thymine N3H protons and adenine H2 protons. These arose from T^3•A^{22}, A^4•T^{21}, A^8•T^{17}, and T^{10}•A^{15} base pairs. As shown in Figure 4A, X^7 N1H exhibited strong NOEs to C^{18} N^4H_a, the complementary nucleotide, and X^7 N^2H. It showed weak NOE cross-peaks to C^6 N^4H_a and Y^{19} N^2H. In contrast, Y^{19} N1H displayed strong NOEs to C^6 N^4H_a and Y^{19} N^2H and weak cross-peaks to C^{18} N^4H_a and X^7 N^2H. A similar pattern of NOE intensities was observed from X^7 N1H and Y^{19} N1H to C^{18} N^4H_b and C^6 N^4H_b. In addition, X^7 N1H exhibited a NOE to A^8 H2 and T^{17} CH_3. The methyl protons of the cross-link had a stronger NOE to X^7 N1H than to Y^{19} N1H. The H_γ protons exhibited weak NOEs to X^7 N1H, whereas H_α exhibited NOEs to both X^7 N1H and Y^{19} N1H.

(b) 5′-Cp-N^2-dG-3′-S-(α)-CH_3-Propyl-5′-Cp-N^2-dG-3′ Cross-Linked Adduct ***8b***. Figure 3B shows the resonances arising from the Watson−Crick hydrogen-bonded imino protons. The complete sequential NOE connectivity was observed between imino protons of the duplex except at the terminal bases. The latter resonances were not observed due to rapid exchange with solvent. The imino resonance arising from the C^6•Y^{19} base pair was assigned at 12.5 ppm; the X^7•C^{18} base pair was assigned at 12.3 ppm. Each imino proton exhibited a strong NOE to the corresponding Watson−Crick hydrogen-bonded amino proton and to the hydrogen-bonded amino proton of the complementary cytosine, as shown in Figure 4B. Further, four strong A•T base parings were present, as evidenced by NOEs between thymine N3H protons and adenine H2 protons. These arose from T^3•A^{22}, A^4•T^{21}, A^8•T^{17}, and T^{10}•A^{15} base pairs. Additional NOEs were observable with a pattern similar to that of the 5′-Cp-N^2-dG-3′-*R*-(α)-CH_3-propyl-5′-Cp-N^2-dG-3′ cross-linked adduct. The H_α proton and methyl protons exhibited stronger cross-peaks to X^7 N1H than to Y^{19} N1H. On the other hand, the H_γ and H_β protons exhibited stronger cross-peaks to Y^{19} N1H than to X^7 N1H.

Assignments of the Cross-Link Protons. (a) 5′-Cp-N^2-dG-3′-R-(α)-CH_3-Propyl-5′-Cp-N^2-dG-3′ Cross-Linked Adduct ***8a***. All cross-link protons were assigned (Figure 5A) from a combination of ^{1}H COSY and NOESY experiments. The CH_3 resonance was observed at 1.03 ppm. It exhibited a COSY cross-peak to a resonance at 3.82 ppm, assigned as the H_α resonance. The H_α proton manifested an additional cross-peak to a resonance at 1.82 ppm, assigned as that arising

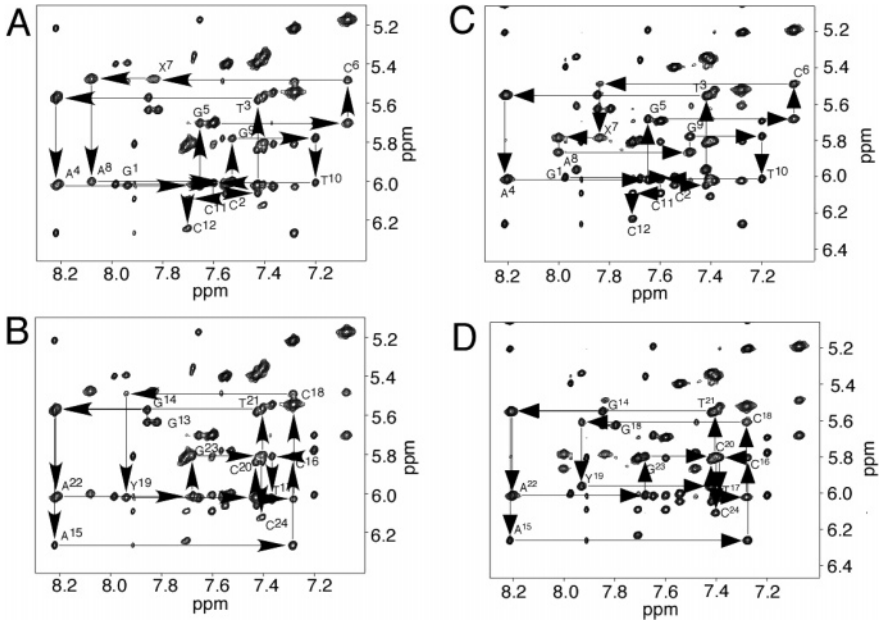

FIGURE 2: Expanded plots of ^{1}H NOESY spectra, showing sequential NOEs from the aromatic to the anomeric protons. (A) Modified strand of the *R*-α-CH_3-γ-OH-1,N^2-propano-2′-deoxyguanosine cross-linked adduct. (B) Complementary strand of the *R*-α-CH_3-γ-OH-1,N^2-propano-2′-deoxyguanosine cross-linked adduct. The NOE mixing time was 150 ms. (C) Modified strand of the *S*-α-CH_3-γ-OH-1,N^2-propano-2′-deoxyguanosine cross-linked adduct. (D) Complementary strand of the *S*-α-CH_3-γ-OH-1,N^2-propano-2′-deoxyguanosine cross-linked adduct. The NOE mixing time was 250 ms. For both the *R*- and *S*-cross-links, the data were acquired at a ^{1}H frequency of 800 MHz. The base positions are indicated at the intranucleotide cross-peaks of the aromatic protons to the anomeric protons.

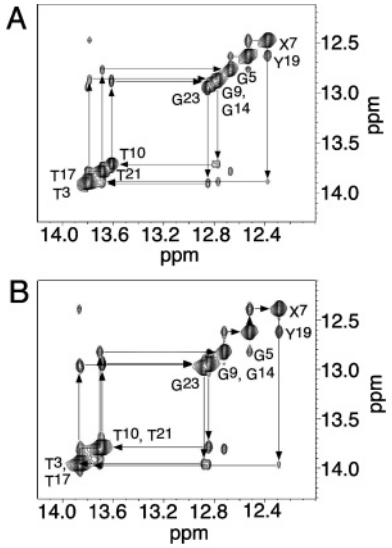

FIGURE 3: Expanded plots of NOESY spectra, showing sequential NOEs for the imino protons. (A) *R*-α-CH_3-γ-OH-1,N^2-Propano-2′-deoxyguanosine cross-linked adduct. (B) *S*-α-CH_3-γ-OH-1,N^2-Propano-2′-deoxyguanosine cross-linked adduct. The data were acquired at a ^{1}H frequency of 800 MHz with a mixing time of 200 ms.

from the $H_{\beta1}$ proton.[2] The $H_{\beta1}$ proton had a strong geminal coupling to a resonance at 1.63 ppm, arising from $H_{\beta2}$, and weak coupling to a resonance at 2.82 ppm, arising from $H_{\gamma2}$. The $H_{\gamma2}$ proton also had a strong geminal coupling to the $H_{\gamma1}$ proton at 3.71 ppm. The $H_{\gamma2}$ and H_α protons were the most deshielded, presumably due to the trans orientation with respect to the hydrogen-bonded N^2H group of deoxyguanosines. All of the anticipated dipolar couplings were observed to other cross-linked protons.

(b) 5′-Cp-N^2-dG-3′-S-(α)-CH_3-Propyl-5′-Cp-N^2-dG-3′ Cross-Linked Adduct ***8b***. All adduct protons were assigned (Figure 5B) from a combination of ^{1}H COSY, TOCSY, and NOESY experiments. The $H_{\beta1} \rightarrow H_{\beta2}$ and $H_{\gamma1} \rightarrow H_{\gamma2}$ geminal couplings exhibited strong DQF-COSY cross-peaks, as did the $CH_3 \rightarrow H_\alpha$ cross-peak. Different chemical shifts were observed as compared to the cross-link with *R*-stereochemistry (Table 1). A major difference was the differential chemical shifts of the H_β protons. The $H_{\beta1}$ proton was observed at 1.09 ppm, while $H_{\beta2}$ was observed at 2.77 ppm. Also, H_α shifted upfield compared to its position in the cross-link with *R*-stereochemistry.

Cross-Link−DNA NOEs. (a) 5′-Cp-N^2-dG-3′-R-(α)-CH_3-Propyl-5′-Cp-N^2-dG-3′ Cross-Linked Adduct ***8a***. The CH_3 protons of the cross-link exhibited strong NOEs to A^8 H2 and A^8 H1′ (Figure 6A). The CH_3 protons exhibited weaker NOEs to X^7 H1′ and C^{20} H1′, and A^8 H2 and H4′. The $H_{\gamma1}$ and $H_{\gamma2}$ protons exhibited stronger NOEs to C^{20} H1′ as compared to the $H_{\beta1}$, $H_{\beta2}$, and H_α protons. Weak NOEs were observed between H_α and A^8 H1′ and X^7 H1′. Overall, this pattern of NOE intensities positioned the methyl group in the 3′ direction with respect to X^7.

(b) 5′-Cp-N^2-dG-3′-S-(α)-CH_3-Propyl-5′-Cp-N^2-dG-3′ Cross-Linked Adduct ***8b***. Figure 6B presents correlations among base protons in base pairs X^7•C^{18} and C^6•Y^{19}, including NOEs to adduct protons. The CH_3 protons exhibited an intense NOE to A^8 H1′ and strong NOEs to A^8 H2 and H4′. Weaker NOEs were observed from the CH_3 protons to X^7 H1′, X^7 H4′, A^8 H3′, and C^{20} H1′. Strong cross-peaks were observed between H_α and $H_{\gamma1}$ and C^{20} H1′. This pattern of NOEs suggested that the CH_3 group was oriented toward the 3′ direction with respect to nucleotide X^7, proximate to A^8 H1′ in the minor groove.

[2] The enantiotopic protons at C_β and C_γ are designated as follows. $H_{\gamma1}$ is the *pro-S* proton at C_γ, $H_{\gamma2}$ the *pro-R* proton at C_γ, $H_{\beta1}$ the *pro-R* proton at C_β, and $H_{\beta2}$ the *pro-S* proton at C_β.

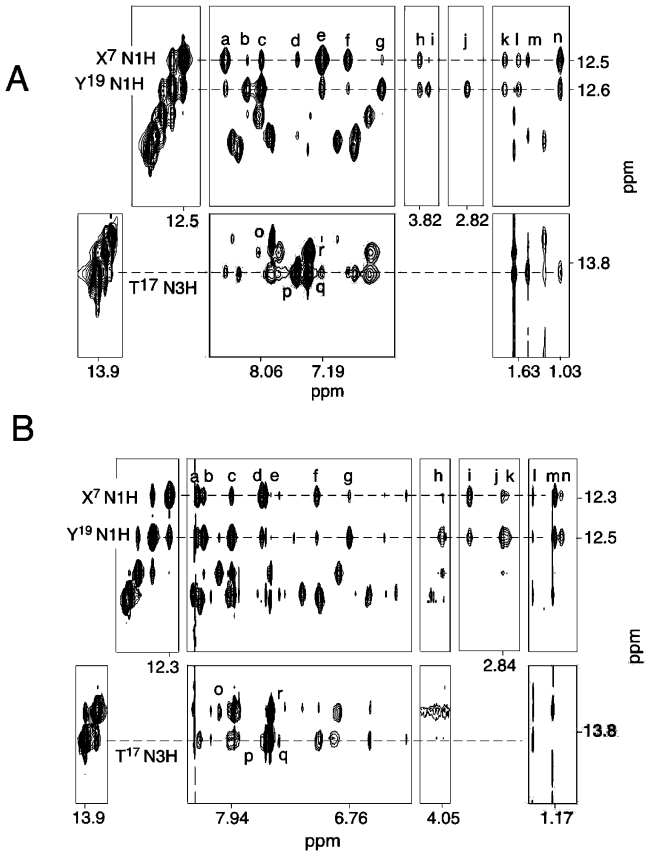

FIGURE 4: (A) *R*-α-CH_3-γ-OH-1,N^2-Propano-2′-deoxyguanosine cross-linked adduct. Tile plot of a NOESY spectrum showing dipolar couplings from selected imino protons to DNA protons. Cross-peak assignments: (a) C^{18} N^4H_a, (b) C^6 N^4H_a, (c) Y^{19} N^2H, (d) A^8 H2, (e) X^7 N^2H, (f) C^{18} N^4H_b, (g) C^6 N^4H_b, (h) X^7 H_α, (i) X^7 $H_{\gamma 1}$, (j) X^7 $H_{\gamma 2}$, (k) X^7 $H_{\beta 1}$, (l) X^7 $H_{\beta 2}$, (m) T^{17} CH_3, (n) X^7 CH_3, (o) A^{15} H2/T^{10} N3H, (p) A^8 H2/T^{17} N3H, (q) A^{22} H2/T^3 N3H, and (r) A^4 H2/T^{21} N3H. The data were acquired with a mixing time of 200 ms. (B) *S*-α-CH_3-γ-OH-1,N^2-Propano-2′-deoxyguanosine cross-linked adduct. Tile plot of a NOESY spectrum showing dipolar coupling from selected imino protons to DNA protons. Cross-peak assignments: (a) C^{18} N^4H_a, (b) C^6 N^4H_a, (c) Y^{19} N^2H, (d) X^7 N^2H, (e) A^8 H2, (f) C^{18} N^4H_b, (g) C^6 N^4H_b, (h) X^7 $H_{\gamma 1}$, (i) X^7 H_α, (j) X^7 $H_{\gamma 2}$, (k) X^7 $H_{\beta 2}$, (l) T^{17} CH_3, (m) X^7 CH_3, (n) X^7 $H_{\beta 1}$, (o) A^{15} H2/T^{10} N3H, (p) A^8 H2/T^{17} N3H, (q) A^{22} H2/T^3 N3H, and (r) A^4 H2/T^{21} N3H. The data were acquired with a mixing time of 250 ms.

Chemical Shift Perturbations. (a) 5′-Cp-N^2-dG-3′-R-(α)-CH_3-Propyl-5′-Cp-N^2-dG-3′ Cross-Linked Adduct ***8a***. Figure S1 (panels A and B) of the Supporting Information compares the chemical shifts of the deoxyribose protons of the cross-linked duplex with those of the corresponding non-cross-linked duplex. The greatest changes were localized to the 5′ neighbor cytosine and X^7 H2′ proton. The other chemical shift perturbations of the base protons were consistently less than 0.1 ppm. The C^6 H1′ and C^{18} H1′ protons each shifted upfield by approximately 0.05 ppm, whereas the X^7 H1′ and Y^{19} H1′ protons were deshielded by approximately 0.02 ppm. These perturbations were similar to those observed for the propyl interstrand cross-link (*42*).

(b) 5′-Cp-N^2-dG-3′-S-(α)-CH_3-Propyl-5′-Cp-N^2-dG-3′ Cross-Linked Adduct ***8b***. Figure S1 (panels C and D) of the Supporting Information compares the chemical shifts of the deoxyribose protons of the cross-linked duplex with those of the corresponding non-cross-linked duplex. The greatest changes were localized to the 5′ neighbor cytosine and X^7 H2′. The largest difference was approximately 0.7 ppm for the 5′ neighbor C^6 H2′. The other chemical shift perturbations of the base protons were consistently less than 0.2 ppm. The C^6 H1′ and C^{18} H1′ protons each shifted upfield by approximately 0.05 ppm, whereas the X^7 H1′ and Y^{19} H1′ protons were deshielded by approximately 0.02 ppm. These chemical shift perturbations were similar to those observed for the propyl interstrand cross-link (*42*).

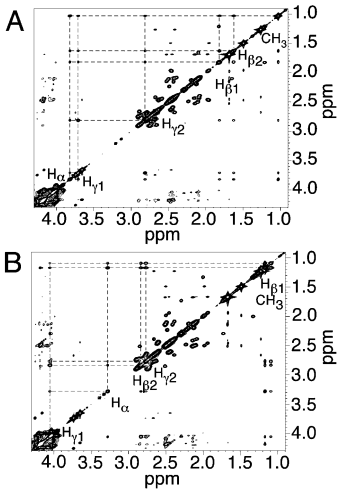

FIGURE 5: Expanded plots of ^1H NOESY spectra showing the assignments of the cross-linked protons. (A) *R*-α-CH_3-γ-OH-1,N^2-Propano-2′-deoxyguanosine cross-linked adduct. (B) *S*-α-CH_3-γ-OH-1,N^2-Propano-2′-deoxyguanosine cross-linked adduct. The data were acquired at a ^1H frequency of 800 MHz with a mixing time of 200 ms.

Table 1: Chemical Shifts (parts per million) of the 5′-Cp-N^2-dG-3′-*R*-(α)-CH_3-Propyl-5′-Cp-N^2-dG-3′ Interstrand DNA Cross-Link **8a** and 5′-Cp-N^2-dG-3′-*S*-(α)-CH_3-Propyl-5′-Cp-N^2-dG-3′ Interstrand DNA Cross-Link **8b**

	X^7 N^2H^a	CH_3	H_α	$H_{\beta 1}$	$H_{\beta 2}$	$H_{\gamma 1}$	$H_{\gamma 2}$	Y^{19} N^2H^a
R-cross-link **8a**	7.19	1.03	3.82	1.82	1.63	3.71	2.82	8.06
S-cross-link **8b**	7.47	1.17	3.28	1.09	2.77	4.06	2.84	7.89

[a] The chemical shift was measured in water at 13 °C.

Torsion Angles. (a) 5′-Cp-N^2-dG-3′-R-(α)-CH_3-Propyl-5′-Cp-N^2-dG-3′ Cross-Linked Adduct ***8a***. The NOE data suggested that all of the glycosyl torsion angles were in the anti conformation. Deoxyribose pseudorotations were estimated from $^3J_{HH}$ coupling constants (*45*). The $^3J_{H1'-H2'}$ and $^3J_{H1'-H2''}$ coupling constants were measured from E-COSY experiments (*46*), while the $^3J_{H2''-H3'}$ and $^3J_{H3'-H4'}$ coupling constants were determined from DQF-COSY experiments. The data were fit to curves relating the coupling constants to the pseudorotation (*P*), sugar pucker amplitude (ϕ), and the percentage *S*-type conformation. The pseudorotation and amplitude ranges were converted to the five dihedral angles $\nu_0-\nu_4$ (*47*). The data were consistent with all deoxyribose pseudorotations being in the *C*2′-endo range. The ^{31}P spectrum exhibited no unusual chemical shifts, suggesting that the backbone was not perturbed.

(b) 5′-Cp-N^2-dG-3′-S-(α)-CH_3-Propyl-5′-Cp-N^2-dG-3′ Cross-Linked Adduct ***8b***. The NOE data suggested that all of the glycosyl torsion angles were in the anti conformation and the deoxyribose sugars were in the *C*2′-endo conformation (*47*). The ^{31}P spectrum exhibited no unusual chemical shifts, suggesting that the backbone was not perturbed.

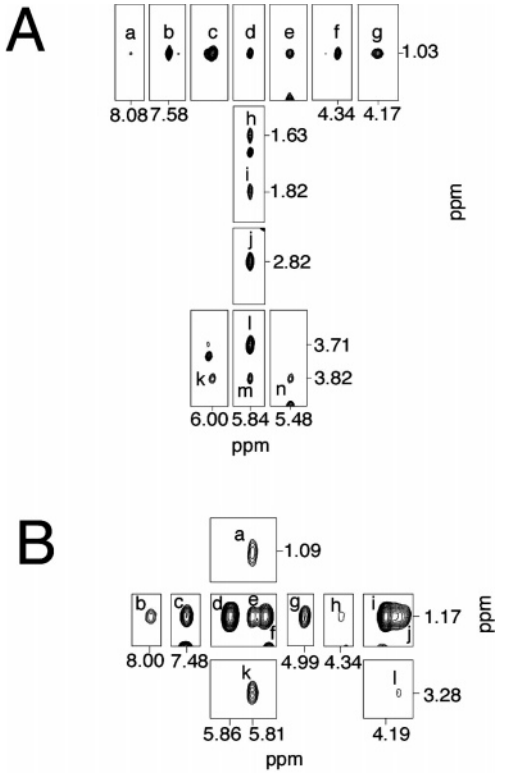

FIGURE 6: Tile plots showing NOEs between the cross-linked protons and DNA protons. (A) *R*-α-CH_3-γ-OH-1,N^2-Propano-2′-deoxyguanosine cross-linked adduct: (a) A^8 H8 → X^7 CH_3, (b) A^8 H2 → X^7 CH_3, (c) A^8 H1′ → X^7 CH_3, (d) C^{20} H1′ → X^7 CH_3, (e) X^7 H1′ → X^7 CH_3, (f) A^8 H4′ → X^7 CH_3, (g) A^8 H5′ → X^7 CH_3, (h) C^{20} H1′ → X^7 $H_{\beta 2}$, (i) C^{20} H1′ → X^7 $H_{\beta 1}$, (j) C^{20} H1′ → X^7 $H_{\gamma 2}$, (k) A^8 H1′ → X^7 H_α, (l) C^{20} H1′ → Y^{19} $H_{\gamma 1}$, (m) C^{20} H1′ → X^7 H_α, and (n) X^7 H1′ → X^7 H_α. The mixing time was 350 ms. (B) *S*-α-CH_3-γ-OH-1,N^2-Propano-2′-deoxyguanosine cross-linked adduct: (a) C^{20} H1′ → X^7 $H_{\beta 1}$, (b) A^8 H8 → X^7 CH_3, (c) A^8 H2 → X^7 CH_3, (d) A^8 H1′ → X^7 CH_3, (e) C^{20} H1′ → X^7 CH_3, (f) X^7 H1′ → X^7 CH_3, (g) A^8 H3′ → X^7 CH_3, (h) X^7 H4′ → X^7 CH_3, (i) A^8 H4′ → X^7 CH_3, (j) C^{20} H4′ → X^7 CH_3 (overlapped), (k) C^{20} H1′ → X^7 H_α, and (l) C^{20} H4′ → X^7 H_α.

Structural Refinement. (a) 5′-Cp-N^2-dG-3′-R-(α)-CH_3-Propyl-5′-Cp-N^2-dG-3′ Cross-Linked Adduct ***8a***. A-Form and B-form DNA starting structures were constructed, with the cross-link between X^7 and Y^{19}. The cross-link was parametrized for AMBER 8.0 as shown in Figure S2 of the Supporting Information. A total of 246 distance restraints were generated from the NOE data using MARDIGRAS (*34*, *48*). In addition, 52 empirical Watson−Crick restraints were incorporated in rMD calculations.

The precision of the rMD calculations was monitored by pairwise rmsd analysis of the emergent structures. Figure S3 (panel A) of the Supporting Information shows a stereoview of structures emerging from the rMD calculations. The rmsd between the A-DNA and B-DNA starting structures was 6.4 Å. The pairwise rmsd between averaged structures from IniA and IniB was 1.4 Å. The final refined structure was compared to the starting A-DNA and B-DNA structures. It exhibited a rmsd of 2.6 Å to the B-DNA starting structure and a rmsd of 4.3 Å to the A-DNA starting structure. This indicated that the convergent structures more closely resembled B-DNA than A-DNA. Detailed results are listed in Table 2.

The accuracies of the structures that emerged from the rMD calculations were evaluated by complete relaxation matrix analysis, using CORMA. Figure S4 (panels A and B) of the Supporting Information presents sixth-root R_1^x residuals at each nucleotide, in comparison with experimental NOE data obtained with a mixing time of 150 ms. The overall R_1^x residual for the cross-linked oligodeoxynucleotide was 7.04×10^{-2}. The overall intranucleotide R_1^x residual was 6.47×10^{-2}, and the overall internucleotide R_1^x residual was 7.72×10^{-2}. These values indicated agreement between the refined structures and the NOESY data.

Table 2: Structural Statistics for the 5′-Cp-N^2-dG-3′-*R*-(α)-CH_3-Propyl-5′-Cp-N^2-dG-3′ Interstrand DNA Cross-Link **8a** and 5′-Cp-N^2-dG-3′-*S*-(α)-CH_3-Propyl-5′-Cp-N^2-dG-3′ Interstrand DNA Cross-Link **8b**

	R-cross-link **8a**	*S*-cross-link **8b**
NMR restraints		
total no. of distance restraints	246	364
no. of interresidue distance restraints	119	164
no. of intraresidue distance restraints	127	200
no. of DNA−adduct proton distance restraints	10	10
no. of adduct proton distance restraints	14	15
no. of H-bonding restraints	52	52
pairwise rmsd (Å) over all atoms		
IniA vs IniB	6.37	6.39
⟨rMDA⟩[a] vs ⟨rMDA⟩	0.53 ± 0.27	0.44 ± 0.23
⟨rMDB⟩[b] vs ⟨rMDB⟩	0.47 ± 0.24	0.26 ± 0.14
$rMDA_{avg}$[c] vs $rMDB_{avg}$[d]	1.38	1.17
$rMDA_{avg}$ vs rMD_{avg}[e]	0.80	0.77
$rMDB_{avg}$ vs rMD_{avg}	1.01	0.74
IniA vs rMD_{avg}	4.34	4.26
IniB vs rMD_{avg}	2.62	2.50

[a] ⟨rMDA⟩ represents the set of five structures that emerged from rMD calculations starting from IniA. [b] ⟨rMDB⟩ represents the set of five structures that emerged from rMD calculations starting from IniB. [c] $rMDA_{avg}$ represents the average structure of all five structures of ⟨rMDA⟩. [d] $rMDB_{avg}$ represents the average structure of all five structures of ⟨rMDB⟩. [e] rMD_{avg} represents the potential energy-minimized average structure of all 10 structures of ⟨rMDA⟩ and ⟨rMDB⟩.

(b) 5′-Cp-N^2-dG-3′-S-(α)-CH_3-Propyl-5′-Cp-N^2-dG-3′ Cross-Linked Adduct ***8b***. A-Form and B-form DNA starting structures were constructed, as described above for cross-linked adduct **8a**. A total of 364 distance restraints were generated from the NOE data using MARDIGRAS (*34*, *48*). A total of 52 empirical Watson−Crick restraints were incorporated in rMD calculations.

Figure S3 (panel B) of the Supporting Information shows a stereoview of convergent structures emerging from the rMD calculations. The rmsd between A-DNA and B-DNA starting structures was 6.4 Å. The pairwise rmsd between averaged structures as compared to the initial A- and B-DNA starting structures was 1.6 Å. The final averaged and energy-minimized structure was compared to the starting structure; a 2.5 Å rmsd was observed between the initial B-form starting structure and rMD_{avg}, while a 4.3 Å rmsd was observed between the initial A-form starting structure and rMD_{avg}. Detailed results are listed in Table 2.

The accuracies of the structures that emerged from the rMD calculations were evaluated by complete relaxation matrix analysis, using CORMA. Figure S4 (panels C and D) of the Supporting Information presents sixth root R_1^x residuals at each nucleotide, in comparison with experimental

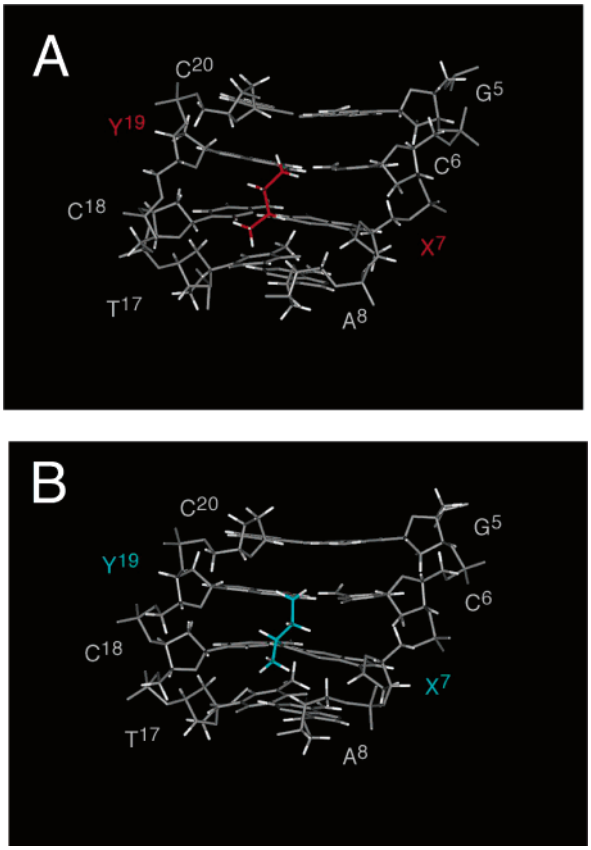

FIGURE 7: Views of the refined structures for the *R*- and *S*-cross-linked oligodeoxynucleotides, shown from the minor groove. (A) *R*-α-CH_3-*γ*-OH-1,N^2-Propano-2′-deoxyguanosine cross-linked adduct (red). (B) *S*-α-CH_3-*γ*-OH-1,N^2-Propano-2′-deoxyguanosine cross-linked adduct (blue).

NOE data obtained with a mixing time of 60 ms. The overall R_1^x residual for the cross-linked oligodeoxynucleotide was 5.70×10^{-2}. The overall intranucleotide R_1^x residual was 5.03×10^{-2}, and the overall internucleotide R_1^x residual was 7.03×10^{-2}. These values indicated agreement between the refined structures and the NOESY data.

Structure of 5′-Cp-N^2-dG-3′-R-(α)-CH_3-Propyl-5′-Cp-N^2-dG-3′ Cross-Linked Adduct ***8a***. Figure 7A shows the refined structure of the interstrand cross-link from the minor groove. The *R*-(α)-CH_3 group is oriented in the 3′ direction with respect to X^7. It faced toward T^{17} in the complementary strand and was centered within the minor groove. This allowed the *R*-(α)-CH_3 group to be easily accommodated within the minor groove. It also allowed the cross-linked oligodeoxynucleotide to maintain Watson−Crick hydrogen bonds and normal base stacking interactions at the tandem cross-linked C^6•Y^{19} and X^7•C^{18} base pairs (Figure 8A). The conformation of the propyl group is shown in a Newman projection in Figure 9A. At the $C_\alpha-C_\beta$ bond, H_α was trans to $H_{\beta1}$ and gauche with respect to $H_{\beta2}$, consistent with the large $H_\alpha \rightarrow H_{\beta1}$ ^3J coupling constant and the smaller $H_\alpha \rightarrow H_{\beta2}$ ^3J coupling constant. At the $C_\beta-C_\gamma$ bond, $H_{\gamma2}$ was trans to $H_{\beta1}$ and gauche with respect to $H_{\beta2}$, consistent with the large $H_{\gamma2} \rightarrow H_{\beta1}$ ^3J coupling constant and the smaller $H_{\gamma2} \rightarrow H_{\beta2}$ ^3J coupling constant.

Structure of 5′-Cp-N^2-dG-3′-S-(α)-CH_3-Propyl-5′-Cp-N^2-dG-3′ Cross-Linked Adduct ***8b***. Figure 7B shows the refined structure of the interstrand cross-link from the minor groove. The *S*-(α)-CH_3 group is oriented in the 3′ direction with respect to X^7. It faced toward A^8 and was within the minor groove. This created a clash between the CH_3 group and the right-handed helical trajectory of the minor groove, as predicted by modeling studies (*25*). Nevertheless, the cross-

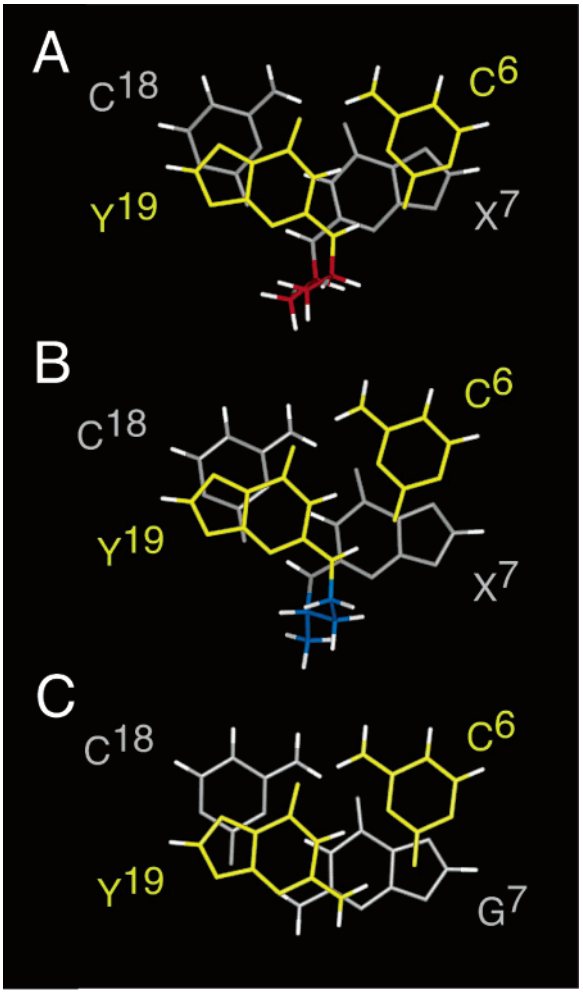

FIGURE 8: (A) Stacking of base pairs C^6•Y^{19} (yellow) and X^7•C^{18} (gray) for the *R*-α-CH_3-*γ*-OH-1,N^2-propano-2′-deoxyguanosine cross-linked adduct (red). (B) Stacking of base pairs C^6•Y^{19} (yellow) and X^7•C^{18} (gray) for the *S*-α-CH_3-*γ*-OH-1,N^2-propano-2′-deoxyguanosine cross-linked adduct (blue). (C) Stacking of base pairs C^6•G^{19} (yellow) and G^7•C^{18} (gray) for the non-cross-linked adduct.

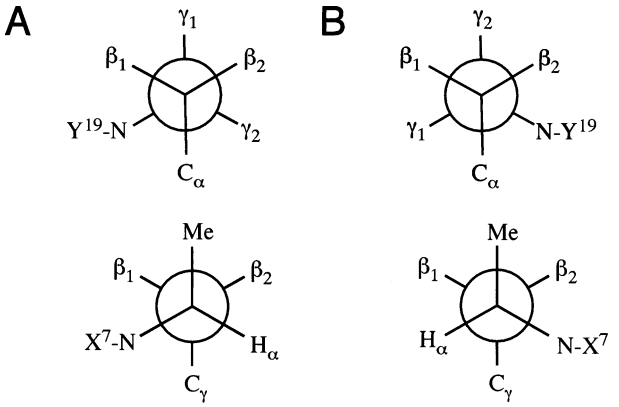

FIGURE 9: (A) Newman projections for the *R*-α-CH_3-*γ*-OH-1,N^2-propano-2′-deoxyguanosine cross-linked adduct: (top) view along the $C_\beta-C_\gamma$ axis and (bottom) view along the $C_\alpha-C_\beta$ axis. (B) Newman projections for the *S*-α-CH_3-*γ*-OH-1,N^2-propano-2′-deoxyguanosine cross-linked adduct: (top) view along the $C_\beta-C_\gamma$ axis and (bottom) view along the $C_\alpha-C_\beta$ axis.

linked oligodeoxynucleotide maintained Watson−Crick hydrogen bonds and reasonable base stacking at the tandem cross-linked C^6•Y^{19} and X^7•C^{18} base pairs, shown in Figure 8B. The conformation of the propyl group is shown in a Newman projection in Figure 9B. At the $C_\alpha-C_\beta$ bond, $H_{\gamma1}$ was trans to $H_{\beta2}$ and gauche with respect to $H_{\beta1}$, consistent with the large $H_{\gamma1} \rightarrow H_{\beta2}$ ^3J coupling constant and the smaller observed $H_{\gamma1} \rightarrow H_{\beta1}$ ^3J coupling constant. At the $C_\beta-C_\gamma$ bond, H_α was trans to $H_{\beta2}$ and gauche with respect to $H_{\beta1}$, consistent with the large $H_\alpha \rightarrow H_{\beta2}$ ^3J coupling constant and the smaller $H_\alpha \rightarrow H_{\beta1}$ ^3J coupling constant. Consequently, the protons of the propyl cross-link were oriented differently than in the corresponding cross-link with *R*-stereochemistry of the CH_3 group, consistent with their differential chemical shifts in the two stereoisomeric cross-links (Figure 5).

DISCUSSION

5′-Cp-*N*^{2}-dG-3′-*R*-(α)-CH_3-propyl-5′-Cp-*N*^{2}-dG-3′ and 5′-Cp-*N*^{2}-dG-3′-*S*-(α)-CH_3-propyl-5′-Cp-*N*^{2}-dG-3′ cross-links **8a** and **8b** provided chemically stable surrogates for carbinolamine cross-links **5a** and **5b** arising from the crotonaldehyde- and acetaldehyde-derived *R*- and *S*-α-CH_3-γ-OH-1,*N*^{2}-propanodeoxyguanosine adducts **2a** and **2b**, respectively, in duplex DNA (*25*). Structural studies on reduced cross-links **8a** and **8b** provided an opportunity to search for an explanation to the observation that interstrand cross-link formation in the 5′-CpG-3′ sequence is dependent upon adduct stereochemistry, favoring the *R*-α-CH_3-γ-OH-1,*N*^{2}-propanodeoxyguanosine adduct **2a**.

Structures of 5′-Cp-N^2*-dG-3′-R-(α)-CH*$_3$*-Propyl-5′-Cp-N*^{2}*-dG-3′ and 5′-Cp-N*^{2}*-dG-3′-S-(α)-CH*$_3$*-Propyl-5′-Cp-N*^{2}*-dG-3′ Cross-Links **8a** and **8b**, Respectively*. The results reveal that 5′-Cp-*N*^{2}-dG-3′-*R*-(α)-CH_3-propyl-5′-Cp-*N*^{2}-dG-3′ cross-link **8a** is thermodynamically more stable than 5′-Cp-*N*^{2}-dG-3′-*S*-(α)-CH_3-propyl-5′-Cp-*N*^{2}-dG-3′ cross-link **8b**. While both cross-links were accommodated within the minor groove of the duplex, with small distortions of DNA structure, the T_m of 5′-Cp-*N*^{2}-dG-3′-*S*-(α)-CH_3-propyl-5′-Cp-*N*^{2}-dG-3′ cross-link **8b** was lower (Figure 1). The differential melting of the two cross-links correlates specifically with the tandem cross-linked C^6•Y^{19} and X^7•C^{18} base pairs. The Watson−Crick hydrogen bonding of these two base pairs is more thermally stable in 5′-Cp-*N*^{2}-dG-3′-*R*-(α)-CH_3-propyl-5′-Cp-*N*^{2}-dG-3′ cross-link **8a** than in 5′-Cp-*N*^{2}-dG-3′-*S*-(α)-CH_3-propyl-5′-Cp-*N*^{2}-dG-3′ cross-link **8b**.

The structural studies suggest that the differential thermal stabilities of the two cross-links are due to stereospecific differences in the conformation of the (α)-CH_3 group. For 5′-Cp-*N*^{2}-dG-3′-*R*-(α)-CH_3-propyl-5′-Cp-*N*^{2}-dG-3′ cross-link **8a**, the (α)-CH_3 group was oriented in the 3′ direction within the minor groove and did not interfere with the right-handed geometry of the minor groove. In contrast, the 3′ orientation of the α-CH_3 group for cross-link **8b** did interfere at X^7 and A^8 with the right-handed geometry of the minor groove. This necessitated the conformational reorganization of cross-link **8b** as compared to cross-link **8a**, with the (α)-CH_3 group placed as far as possible from the floor of the minor groove at X^7. The differential patterns of ^3J coupling constants in the ^{1}H NMR spectra corroborated the differential conformations of the three-carbon cross-links. For 5′-Cp-*N*^{2}-dG-3′-*R*-(α)-CH_3-propyl-5′-Cp-*N*^{2}-dG-3′ cross-link **8a**, the $H_{\beta1} \rightarrow H_{\gamma2}$ and $H_\alpha \rightarrow H_{\beta1}$ cross-peaks exhibited large ^3J coupling constants consistent with their trans orientation. In addition, for cross-link **8b**, the $H_{\beta2} \rightarrow H_{\gamma1}$ and $H_\alpha \rightarrow H_{\beta2}$ cross-peaks exhibited large ^3J coupling constants consistent with their trans orientation. Likewise, the different chemical shifts of the propyl protons in the stereoisomeric cross-links were consistent with the conclusion that the corresponding protons in the two cross-links were in different environments.

Molecular modeling had predicted that carbinolamine cross-links **5a** and **5b**, with sp^3 hybridization at the γ-carbon, allowed the tandem cross-linked C^6•Y^{19} and X^7•C^{18} base pairs to maintain Watson−Crick hydrogen bonding (*25*). In contrast, dehydration of the carbinolamine to the imine (Schiff base) cross-link would result in sp^2 hybridization and loss of Watson−Crick hydrogen bonding. 5′-Cp-*N*^{2}-dG-3′-*R*-(α)-CH_3-propyl-5′-Cp-*N*^{2}-dG-3′ cross-link **8a** and 5′-Cp-*N*^{2}-dG-3′-*S*-(α)-CH_3-propyl-5′-Cp-*N*^{2}-dG-3′ cross-link **8b** lack the γ-OH group present in the native cross-links. However, it may be inferred from the results presented here that the sp^3 hybridization at the γ-carbon of the cross-link does allow the exocyclic amine proton at Y^{19} to participate in Watson−Crick hydrogen bonding, with minimal perturbation of the DNA duplex, irrespective of *R*- versus *S*-stereochemistry at the (α)-CH_3 group (Figure 8). In both reduced cross-links **8a** and **8b**, the exocyclic amine protons at both X^7 and Y^{19} were observed in the NMR spectra, and for both reduced cross-links **8a** and **8b**, the exocyclic amine protons at both X^7 and Y^{19} exhibited NOEs to the corresponding X^7 N1H and Y^{19} N1H imino protons, consistent with the conclusion that they were participating in hydrogen bonds. This is indicative of Watson−Crick hydrogen bonds at both C^6•Y^{19} and X^7•C^{18} base pairs, for both reduced cross-links **8a** and **8b**. This is consistent with studies of other *N*^{2}-dG adducts such as those arising from mitomycin C, anthramycin, and benzo[*a*]pyrene diol epoxides that leave the deoxyguanosine exocyclic amine proton available to participate in Watson−Crick hydrogen bonding (*50*−*52*).

Comparison with the 5′-Cp-N^2*-dG-3′-Propyl-5′-Cp-N*^{2}*-dG-3′ Cross-Link*. A similar strategy was used by Dooley et al. (*42*, *53*) to examine the reduced 5′-Cp-*N*^{2}-dG-3′-propyl-5′-Cp-*N*^{2}-dG-3′ and 5′-*N*^{2}-dGpC-3′-propyl-5′-*N*^{2}-dGpC-3′ cross-links in the 5′-CpG-3′ versus 5′-GpC-3′ sequences. In the 5′-CpG-3′ sequence, the structure of Dooley et al. (*42*) differed from those of the 5′-Cp-*N*^{2}-dG-3′-*R*-(α)-CH_3-propyl-5′-Cp-*N*^{2}-dG-3′ cross-link **8a** and 5′-Cp-*N*^{2}-dG-3′-*S*-(α)-CH_3-propyl-5′-Cp-*N*^{2}-dG-3′ cross-link **8b** reported herein. In the 5′-Cp-*N*^{2}-dG-3′-propyl-5′-Cp-*N*^{2}-dG-3′ cross-link, their three-carbon cross-link was accommodated by unwinding of the duplex at the cross-linked base pairs to produce a bulge. The tethered guanines were approximately in the same plane. Consequently, Watson−Crick hydrogen bonding was disrupted at the tandem cross-linked base pairs. The formation of a bulge accommodated the extended chain conformation of the linker between the two deoxyguanosines in the 5′-CpG-3′ sequence. In the extended chain conformation, the exocyclic nitrogens of each deoxyguanosine were in an anti orientation with respect to their respective γ-carbon atoms of the propyl cross-link (*42*). For the 5′-Cp-*N*^{2}-dG-3′-*R*-(α)-CH_3-propyl-5′-Cp-*N*^{2}-dG-3′ cross-link **8a** and 5′-Cp-*N*^{2}-dG-3′-*S*-(α)-CH_3-propyl-5′-Cp-*N*^{2}-dG-3′ cross-link **8b**, the exocyclic nitrogens of each deoxyguanosine were instead in the gauche orientation with respect to their respective γ-carbon

atoms of the propyl cross-link (Figure 9). Molecular modeling suggested that the presence of either stereoisomer of the (α)-CH_3 group created steric strain in the extended chain conformation, which may explain the observed gauche orientation of the exocyclic nitrogens of each deoxyguanosine with respect to their respective Ω-carbon atoms in the crotonaldehyde-derived cross-links.

*Kinetics of Interstrand Cross-Link Formation by the R- and S-α-CH_3-γ-OH-PdG Adducts (**2a** and **2b**, respectively).* In addition to being energetically disfavored with respect to the interstrand cross-link formed by *R*-α-CH_3-γ-OH-PdG adduct **2a**, the rate of cross-link formation by *S*-α-CH_3-γ-OH-PdG adduct **2b** is slower. Twenty days after annealing 5′-d(GCTAGCXAGTCC)-3′•5′-d(GGACTCYCTAGC)-3′ (X = *R*- or *S*-*a*-CH_3-γ-^{13}C-OH-PdG; Y = $^{15}N^2$-dG) at pH 7 and 37 °C, spectroscopically detectable amounts of an interstrand carbinolamine cross-link were observed only for *R*-α-CH_3-γ-OH-PdG adduct **2a** (*25*). However, treatment of the oligodeoxynucleotide containing *S*-*a*-CH_3-γ-OH-PdG adduct **2b** with $NaCNBH_3$ successfully trapped the reduced interstrand cross-link **8b** (*23*), suggesting that imine cross-link **6b** was in fact present, below the level of NMR detection. Subsequent ^{13}C HSQC NMR studies, in which the sample was monitored at 37 °C for 70 days, revealed the presence of interstrand 5′-CpG-3′ carbinolamine cross-link **5b** derived from *S*-α-CH_3-γ-^{13}C-OH-PdG adduct **2b**. Thus, at pH 7 and 37 °C, 20 days was not sufficient to allow the duplex containing *S*-α-CH_3-γ-^{13}C-OH-PdG adduct **2b** to reach equilibrium.

Previous studies revealed a structural basis for the slow rate of interstrand cross-link formation by *S*-α-CH_3-γ-OH-PdG adduct **2b** (*54*). Within the minor groove, the aldehyde moiety of adduct **3b** is oriented in the 3′ direction, while the 1(*S*)-methyl group is oriented in the 5′ direction. This positioned the aldehyde distal to the G^{19} amino group, hindering formation of the 5′-CpG-3′ interstrand cross-link (*54*). Thus, we conclude that the formation of interstrand cross-links by N^2-(*S*-α-CH_3-γ-OH-1,N^2-propano-2′)-dG adduct **2b** is not only energetically disfavored but also kinetically disfavored. Both the energetics and the kinetics of cross-link formation are modulated by stereochemistry at the (α)-CH_3 group.

Biological Implications. The crotonaldehyde- and acetaldehyde-derived *R*- and *S*-α-CH_3-γ-OH-1,N^2-propanodeoxyguanosine adducts **2a** and **2b** have both been isolated from mammalian tissues, including human cells (*11*−*13*). Both are thought to contribute to the etiology of human mutagenesis and cancer. When DNA containing adducts **2a** and **2b** was introduced into human xeroderma pigmentosum A (XPA) cells and examined with respect to replication (*55*), the major miscoding events in the XPA cells for both adducts were G → T transversions, with G → A transitions also being observed for adduct **2a**, whereas G → C transversions were the second most common events for adduct **2b**. The site-specific mutagenesis of adducts **2a** and **2b** has also been examined in COS-7 cells, also showing primarily G → T transversions (*56*). It is generally thought that the propensity of cyclic adducts **2a** or **2b** to undergo ring opening to N^2-(3-oxopropyl)-dG aldehydes **3a** and **3b** (Chart 1) facilitates lesion bypass, as reported for the acrolein-derived γ-OH-PdG adduct (*57*−*61*). On the other hand, in duplex DNA, incomplete conversion of crotonaldehyde-derived adducts **2a** and **2b** to aldehydes **3a** and **3b** or hydrated aldehydes **4a** and **4b**, respectively, may block DNA replication, possibly reducing their mutagenicity. The formation of interstrand carbinolamine cross-link **5a** by *R*-α-CH_3-γ-OH-1,N^2-propanodeoxyguanosine adduct **2a** might also block DNA replication, and thus reduce its mutagenicity as compared to that of *S*-α-CH_3-γ-OH-1,N^2-propanodeoxyguanosine adduct **2b**. The equilibrium chemistry of adducts **2a** and **2b** and, in particular, the chemical stability of carbinolamine cross-link **5a** (Chart 1), within DNA replication or repair complexes, are of considerable interest; Liu et al. (*26*) report that cross-links **5a** and **5b** were stable during construction of site-specifically modified plasmids but concluded that in *E. coli*, proficient nucleotide excision repair was absolutely required to repair cross-link **8a**. Thus, *E. coli* transformants obtained using cross-links **5a** and **5b** were interpreted as arising from some proportion of native cross-links that had reverted to the respective monoadducts. However, in nucleotide excision repair-deficient human XPA cells, residual repair of cross-link **8a** was observed (*26*), which suggested the presence of a replication-coupled NER-independent cross-link repair pathway (*62*), e.g., the proposed ERCC1-XPF endonuclease replication fork cross-link repair pathway (*63*, *64*). In XPA cells, the primary mutations induced as a consequence of error-prone repair of reduced cross-link **8a** were low levels of G → T transversions targeting the cross-linked dG in the lagging strand template (*26*). The specific polymerases responsible for trans-lesion synthesis remain to be identified, but Y-family polymerase η (*65*) and pol ζ (*66*, *67*) are candidates. Washington et al. (*68*, *69*) showed that Y-polymerase pol ι in conjunction with pol κ, or Rev 1 in combination with pol ζ, could efficiently bypass the acrolein-derived γ-OH-PdG adduct. Minko et al. (*70*) showed that pol η could bypass the γ-OH-PdG adduct to a lesser extent. It seems plausible that these error-prone polymerases might also bypass equilibrium mixtures of crotonaldehyde- and acetaldehyde-derived monoadducts **2a**, **3a**, and **4a** or **2b**, **3b**, and **4b** or partially excised intermediates arising from replication-coupled repair of interstrand cross-links **5a** and **5b**.

ACKNOWLEDGMENT

We thank Dr. Jarrod Smith for suggestions regarding AMBER calculations. Portions of this work were presented at the 230th National Meeting of the American Chemical Society, August 28 to September 1, 2005, Washington, D.C.

SUPPORTING INFORMATION AVAILABLE

Nonexchangeable ^{1}H chemical shifts for 5′-d(GCTAGCX-AGTCC)-3′•5′-(GGACTCYCTAGC)-3′ containing interstrand cross-link **8a** (Table S1), nonexchangeable ^{1}H chemical shifts for 5′-d(GCTAGCXAGTCC)-3′•5′-(GGACTCYCT-AGC)-3′ containing interstrand cross-link **8b** (Table S2), exchangeable ^{1}H chemical shifts for the oligodeoxynucleotide containing cross-link **8a** (Table S3), exchangeable ^{1}H chemical shifts for the oligodeoxynucleotide containing cross-link **8b** (Table S4), NOE restraints utilized in rMD calculations for the oligodeoxynucleotide containing cross-link **8a** (Table S5), NOE restraints utilized in rMD calculations for the oligodeoxynucleotide containing cross-link **8b** (Table S6), chemical shift differences of nonexchangeable aromatic

protons between cross-linked oligodeoxynucleotides **8a** and **8b** and the non-cross-linked oligodeoxynucleotide (Figure S1), parametrization of cross-link **8a** in the AMBER 8.0 force field (Figure S2), stereoviews of structures that emerged from randomly seeded rMD calculations of oligodeoxynucleotides containing cross-links **8a** and **8b** (Figure S3), and complete relaxation matrix calculations on average structures that emerged from randomly seeded rMD calculations of the oligodeoxynucleotides containing cross-links **8a** and **8b**, showing sixth-root residuals (R_1^x) for each nucleotide (Figure S4). This material is available free of charge via the Internet at http://pubs.acs.org.

REFERENCES

1. Czerny, C., Eder, E., and Runger, T. M. (1998) Genotoxicity and mutagenicity of the α,*β*-unsaturated carbonyl compound crotonaldehyde (butenal) on a plasmid shuttle vector, *Mutat. Res. 407*, 125−134.
2. Chung, F. L., Tanaka, T., and Hecht, S. S. (1986) Induction of liver tumors in F344 rats by crotonaldehyde, *Cancer Res. 46*, 1285−1289.
3. Chung, F. L., and Hecht, S. S. (1983) Formation of cyclic 1,N^2-adducts by reaction of deoxyguanosine with α-acetoxy-N-nitrosopyrrolidine, 4-(carbethoxynitrosamino)butanal, or crotonaldehyde, *Cancer Res. 43*, 1230−1235.
4. Eder, E., Schuler, D., and Budiawan (1999) Cancer risk assessment for crotonaldehyde and 2-hexenal: An approach, *IARC Sci. Publ. 150*, 219−232.
5. Chung, F. L., Zhang, L., Ocando, J. E., and Nath, R. G. (1999) Role of 1,N^2-propanodeoxyguanosine adducts as endogenous DNA lesions in rodents and humans, *IARC Sci. Publ. 150*, 45−54.
6. Wang, M., McIntee, E. J., Cheng, G., Shi, Y., Villalta, P. W., and Hecht, S. S. (2000) Identification of DNA adducts of acetaldehyde, *Chem. Res. Toxicol. 13*, 1149−1157.
7. Wang, M., McIntee, E. J., Cheng, G., Shi, Y., Villalta, P. W., and Hecht, S. S. (2000) Identification of paraldol-deoxyguanosine adducts in DNA reacted with crotonaldehyde, *Chem. Res. Toxicol. 13*, 1065−1074.
8. Wang, M., McIntee, E. J., Cheng, G., Shi, Y., Villalta, P. W., and Hecht, S. S. (2001) A Schiff base is a major DNA adduct of crotonaldehyde, *Chem. Res. Toxicol. 14*, 423−430.
9. International Agency for Research on Cancer (1999) Re-evaluation of some organic chemicals, hydrazine and hydrogen peroxide, IRC Monographs on the Evaluation of Carcinogenic Risks to Humans, *IARC Sci. Publ. 71*, 109−125.
10. Lao, Y., and Hecht, S. S. (2005) Synthesis and properties of an acetaldehyde-derived oligonucleotide interstrand cross-link, *Chem. Res. Toxicol. 18*, 711−721.
11. Chung, F. L., Nath, R. G., Nagao, M., Nishikawa, A., Zhou, G. D., and Randerath, K. (1999) Endogenous formation and significance of 1,N^2-propanodeoxyguanosine adducts, *Mutat. Res. 424*, 71−81.
12. Budiawan and Eder, E. (2000) Detection of 1,N^2-propanodeoxyguanosine adducts in DNA of Fischer 344 rats by an adapted ^{32}P-post-labeling technique after per os application of crotonaldehyde, *Carcinogenesis 21*, 1191−1196.
13. Zhang, S., Villalta, P. W., Wang, M., and Hecht, S. S. (2006) Analysis of crotonaldehyde- and acetaldehyde-derived 1,N^2-propanodeoxyguanosine adducts in DNA from human tissues using liquid chromatography electrospray ionization tandem mass spectrometry, *Chem. Res. Toxicol. 19*, 1386−1392.
14. Nath, R. G., and Chung, F. L. (1994) Detection of exocyclic 1,N^2-propanodeoxyguanosine adducts as common DNA lesions in rodents and humans, *Proc. Natl. Acad. Sci. U.S.A. 91*, 7491−7495.
15. Nath, R. G., Ocando, J. E., and Chung, F. L. (1996) Detection of 1,N^2-propanodeoxyguanosine adducts as potential endogenous DNA lesions in rodent and human tissues, *Cancer Res. 56*, 452−456.
16. Treitman, R. D., Burgess, W. A., and Gold, A. (1980) Air contaminants encountered by firefighters, *Am. Ind. Hyg. Assoc. J. 41*, 796−802.
17. Izard, C., Valadaud-Barrieu, D., Fayeulle, J. P., and Testa, A. (1980) [Effect of smoking-machine parameters on the genotoxic activity of cigarette gas phase, estimated on human lymphocyte and yeast], *Mutat. Res. 77*, 341−344.
18. Chung, F. L., Chen, H. J., and Nath, R. G. (1996) Lipid peroxidation as a potential endogenous source for the formation of exocyclic DNA adducts, *Carcinogenesis 17*, 2105−2111.
19. Hecht, S. S., Upadhyaya, P., and Wang, M. (1999) Reactions of α-acetoxy-N-nitrosopyrrolidine and crotonaldehyde with DNA, *IARC Sci. Publ. 150*, 147−154.
20. Kozekov, I. D., Nechev, L. V., Sanchez, A., Harris, C. M., Lloyd, R. S., and Harris, T. M. (2001) Interchain cross-linking of DNA mediated by the principal adduct of acrolein, *Chem. Res. Toxicol. 14*, 1482−1485.
21. Nechev, L. V., Kozekov, I., Harris, C. M., and Harris, T. M. (2001) Stereospecific synthesis of oligonucleotides containing crotonaldehyde adducts of deoxyguanosine, *Chem. Res. Toxicol. 14*, 1506−1512.
22. Nechev, L. V., Zhang, M., Tsarouhtsis, D., Tamura, P. J., Wilkinson, A. S., Harris, C. M., and Harris, T. M. (2001) Synthesis and characterization of nucleosides and oligonucleotides bearing adducts of butadiene epoxides on adenine N^6 and guanine N^2, *Chem. Res. Toxicol. 14*, 379−388.
23. Kozekov, I. D., Nechev, L. V., Moseley, M. S., Harris, C. M., Rizzo, C. J., Stone, M. P., and Harris, T. M. (2003) DNA interchain cross-links formed by acrolein and crotonaldehyde, *J. Am. Chem. Soc. 125*, 50−61.
24. Kurtz, A. J., and Lloyd, R. S. (2003) 1,N^2-Deoxyguanosine adducts of acrolein, crotonaldehyde, and trans-4-hydroxynonenal cross-link to peptides via Schiff base linkage, *J. Biol. Chem. 278*, 5970−5976.
25. Cho, Y. J., Wang, H., Kozekov, I. D., Kurtz, A. J., Jacob, J., Voehler, M., Smith, J., Harris, T. M., Lloyd, R. S., Rizzo, C. J., and Stone, M. P. (2006) Stereospecific formation of interstrand carbinolamine DNA cross-links by crotonaldehyde- and acetaldehyde-derived α-CH_3-*γ*-OH-1,N^2-propano-2′-deoxyguanosine adducts in the 5′-CpG-3′ sequence, *Chem. Res. Toxicol. 19*, 195−208.
26. Liu, X., Lao, Y., Yang, I. Y., Hecht, S. S., and Moriya, M. (2006) Replication-coupled repair of crotonaldehyde/acetaldehyde-induced guanine-guanine interstrand cross-links and their mutagenicity, *Biochemistry 45*, 12898−12905.
27. Borer, P. N. (1975) *Handbook of Biochemistry and Molecular Biology*, 1st ed., CRC Press, Cleveland, OH.
28. Campbell, T. G., and Urbach, F. L. (1973) Synthesis and characterization of nickel(II) complexes of neutral, tetradentate Schiff-base ligands derived from 1,3-diamines, *Inorg. Chem. 12*, 1836−1840.
29. Piotto, M., Saudek, V., and Sklenar, V. (1992) Gradient-tailored excitation for single-quantum NMR spectroscopy of aqueous solutions, *J. Biomol. NMR 2*, 661−665.
30. Piantini, U., Sorensen, O. W., and Ernst, R. R. (1982) Multiple quantum filters for elucidating NMR coupling networks, *J. Am. Chem. Soc. 104*, 6800−6801.
31. Rance, M., Sorensen, O. W., Bodenhausen, G., Wagner, G., Ernst, R. R., and Wuthrich, K. (1983) Improved spectral resolution in COSY ^{1}H NMR spectra of proteins via double quantum filtering, *Biochem. Biophys. Res. Commun. 177*, 479−485.
32. Delaglio, F., Grzesiek, S., Vuister, G. W., Zhu, G., Pfeifer, J., and Bax, A. (1995) NMRPipe: A multidimensional spectral processing system based on UNIX pipes, *J. Biomol. NMR 6*, 277−293.
33. Keepers, J. W., and James, T. L. (1984) A theoretical study of distance determination from NMR. Two-dimensional nuclear Overhauser effect spectra, *J. Magn. Reson. 57*, 404−426.
34. Borgias, B. A., and James, T. L. (1990) MARDIGRAS: A procedure for matrix analysis of relaxation for discerning geometry of an aqueous structure, *J. Magn. Reson. 87*, 475−487.
35. Liu, H., Tonelli, M., and James, T. L. (1996) Correcting NOESY cross-peak intensities for partial relaxation effects enabling accurate distance information, *J. Magn. Reson., Ser. B 111*, 85−89.
36. Case, D. A., Pearlman, D. A., Caldwell, J. W., Cheatham, T. E., III, Wang, J., Ross, W. S., Simmerling, C. L., Darden, T. A., Merz, K. M., Stanton, R. V., Cheng, A. L., Vincent, J. J., Crowley, M., Tsui, V., Gohlke, H., Radmer, R. J., Duan, Y., Pitera, J., Massova, I., Seibel, G. L., Singh, U. C., Weiner, P. K., and Kollman, P. A. (2002) *AMBER 8.0*, University of California, San Francisco.
37. Arnott, S., and Hukins, D. W. L. (1972) Optimised parameters for A-DNA and B-DNA, *Biochem. Biophys. Res. Commun. 47*, 1504−1509.

38. Frisch, M. J., Trucks, G. W., et al. (1998) *GAUSSIAN98*, Gaussian, Inc., Pittsburgh, PA.
39. Bashford, D., and Case, D. A. (2000) Generalized Born models of macromolecular solvation effects, *Annu. Rev. Phys. Chem. 51*, 129−152.
40. Tsui, V., and Case, D. A. (2000) Theory and applications of the generalized Born solvation model in macromolecular simulations, *Biopolymers 56*, 275−291.
41. Lu, X. J., and Olson, W. K. (2003) 3DNA: A software package for the analysis, rebuilding and visualization of three-dimensional nucleic acid structures, *Nucleic Acids Res. 31*, 5108−5121.
42. Dooley, P. A., Tsarouhtsis, D., Korbel, G. A., Nechev, L. V., Shearer, J., Zegar, I. S., Harris, C. M., Stone, M. P., and Harris, T. M. (2001) Structural studies of an oligodeoxynucleotide containing a trimethylene interstrand cross-link in a 5′-(CpG) motif: Model of a malondialdehyde cross-link, *J. Am. Chem. Soc. 123*, 1730−1739.
43. Patel, D. J., Shapiro, L., and Hare, D. (1987) DNA and RNA: NMR studies of conformations and dynamics in solution, *Q. Rev. Biophys. 20*, 35−112.
44. Reid, B. R. (1987) Sequence-specific assignments and their use in NMR studies of DNA structure, *Q. Rev. Biophys. 20*, 2−28.
45. Salazar, M., Fedoroff, O. Y., Miller, J. M., Ribeiro, N. S., and Reid, B. R. (1993) The DNA strand in DNA:RNA hybrid duplexes is neither B-form nor A-form in solution, *Biochemistry 32*, 4207−4215.
46. Griesinger, G., Sorensen, O. W., and Ernst, R. R. (1985) Two-dimensional correlation of connected NMR transitions, *J. Am. Chem. Soc. 107*, 6394−6396.
47. Kim, S. G., Lin, L. J., and Reid, B. R. (1992) Determination of nucleic acid backbone conformation by ^{1}H NMR, *Biochemistry 31*, 3564−3574.
48. Liu, H., Spielmann, H. P., Ulyanov, N. B., Wemmer, D. E., and James, T. L. (1995) Interproton distance bounds from 2D NOE intensities: Effect of experimental noise and peak integration errors, *J. Biomol. NMR 6*, 390−402.
49. Cho, Y. J., Kim, H. Y., Huang, H., Slutsky, A., Minko, I. G., Wang, H., Nechev, L. V., Kozekov, I. D., Kozekova, A., Tamura, P., Jacob, J., Voehler, M., Harris, T. M., Lloyd, R. S., Rizzo, C. J., and Stone, M. P. (2005) Spectroscopic characterization of interstrand carbinolamine cross-links formed in the 5′-CpG-3′ sequence by the acrolein-derived γ-OH-1,N^2-propano-2′-deoxyguanosine DNA adduct, *J. Am. Chem. Soc. 127*, 17686−17696.
50. Kozack, R. E., and Loechler, E. L. (1997) Molecular modeling of the conformational complexity of (+)-anti-B[a]PDE-adducted DNA using simulated annealing, *Carcinogenesis 18*, 1585−1593.
51. Kopka, M. L., Goodsell, D. S., Baikalov, I., Grzeskowiak, K., Cascio, D., and Dickerson, R. E. (1994) Crystal structure of a covalent DNA-drug adduct: Anthramycin bound to C-C-A-A-C-G-T-T-G-G and a molecular explanation of specificity, *Biochemistry 33*, 13593−13610.
52. Norman, D., Live, D., Sastry, M., Lipman, R., Hingerty, B. E., Tomasz, M., Broyde, S., and Patel, D. J. (1990) NMR and computational characterization of mitomycin cross-linked to adjacent deoxyguanosines in the minor groove of the d(T-A-C-G-T-A):d(T-A-C-G-T-A) duplex, *Biochemistry 29*, 2861−2875.
53. Dooley, P. A., Zhang, M., Korbel, G. A., Nechev, L. V., Harris, C. M., Stone, M. P., and Harris, T. M. (2003) NMR determination of the conformation of a trimethylene interstrand cross-link in an oligodeoxynucleotide duplex containing a 5′-d(GpC) motif, *J. Am. Chem. Soc. 125*, 62−72.
54. Cho, Y. J., Wang, H., Kozekov, I. D., Kozekova, A., Kurtz, A. J., Jacob, J., Voehler, M., Smith, J., Harris, T. M., Rizzo, C. J., Lloyd, R. S., and Stone, M. P. (2006) Orientation of the crotonaldehyde-derived N^2-[3-oxo-1(S)-methyl-propyl]-dG DNA adduct hinders interstrand cross-link formation in the 5′-CpG-3′ sequence, *Chem. Res. Toxicol. 19*, 1019−1029.
55. Stein, S., Lao, Y., Yang, I. Y., Hecht, S. S., and Moriya, M. (2006) Genotoxicity of acetaldehyde- and crotonaldehyde-induced 1,N^2-propanodeoxyguanosine DNA adducts in human cells, *Mutat. Res. 608*, 1−7.
56. Fernandes, P. H., Kanuri, M., Nechev, L. V., Harris, T. M., and Lloyd, R. S. (2005) Mammalian cell mutagenesis of the DNA adducts of vinyl chloride and crotonaldehyde, *Environ. Mol. Mutagen. 45*, 455−459.
57. Yang, I. Y., Hossain, M., Miller, H., Khullar, S., Johnson, F., Grollman, A., and Moriya, M. (2001) Responses to the major acrolein-derived deoxyguanosine adduct in *Escherichia coli*, *J. Biol. Chem. 276*, 9071−9076.
58. Yang, I. Y., Chan, G., Miller, H., Huang, Y., Torres, M. C., Johnson, F., and Moriya, M. (2002) Mutagenesis by acrolein-derived propanodeoxyguanosine adducts in human cells, *Biochemistry 41*, 13826−13832.
59. Yang, I.-Y., Johnson, R., Grollman, A. P., and Moriya, M. (2002) Genotoxic mechanism for the major acrolein-derived deoxyguanosine adduct in human cells, *Chem. Res. Toxicol. 15*, 160−164.
60. Sanchez, A. M., Minko, I. G., Kurtz, A. J., Kanuri, M., Moriya, M., and Lloyd, R. S. (2003) Comparative evaluation of the bioreactivity and mutagenic spectra of acrolein-derived α-HOPdG and γ-HOPdG regioisomeric deoxyguanosine adducts, *Chem. Res. Toxicol. 16*, 1019−1028.
61. VanderVeen, L. A., Hashim, M. F., Nechev, L. V., Harris, T. M., Harris, C. M., and Marnett, L. J. (2001) Evaluation of the mutagenic potential of the principal DNA adduct of acrolein, *J. Biol. Chem. 276*, 9066−9070.
62. Bessho, T. (2003) Induction of DNA replication-mediated double strand breaks by psoralen DNA interstrand cross-links, *J. Biol. Chem. 278*, 5250−5254.
63. Kuraoka, I., Kobertz, W. R., Ariza, R. R., Biggerstaff, M., Essigmann, J. M., and Wood, R. D. (2000) Repair of an interstrand DNA cross-link initiated by ERCC1-XPF repair/recombination nuclease, *J. Biol. Chem. 275*, 26632−26636.
64. Niedernhofer, L. J., Odijk, H., Budzowska, M., van Drunen, E., Maas, A., Theil, A. F., de Wit, J., Jaspers, N. G., Beverloo, H. B., Hoeijmakers, J. H., and Kanaar, R. (2004) The structure-specific endonuclease ERCC1-XPF is required to resolve DNA interstrand cross-link-induced double-strand breaks, *Mol. Cell. Biol. 24*, 5776−5787.
65. Zheng, H., Wang, X., Warren, A. J., Legerski, R. J., Nairn, R. S., Hamilton, J. W., and Li, L. (2003) Nucleotide excision repair- and polymerase η-mediated error-prone removal of mitomycin C interstrand cross-links, *Mol. Cell. Biol. 23*, 754−761.
66. Shen, X., Jun, S., O'Neal, L. E., Sonoda, E., Bemark, M., Sale, J. E., and Li, L. (2006) REV3 and REV1 play major roles in recombination-independent repair of DNA interstrand cross-links mediated by monoubiquitinated proliferating cell nuclear antigen (PCNA), *J. Biol. Chem. 281*, 13869−13872.
67. Sarkar, S., Davies, A. A., Ulrich, H. D., and McHugh, P. J. (2006) DNA interstrand crosslink repair during G1 involves nucleotide excision repair and DNA polymerase ζ, *EMBO J. 25*, 1285−1294.
68. Washington, M. T., Minko, I. G., Johnson, R. E., Wolfle, W. T., Harris, T. M., Lloyd, R. S., Prakash, S., and Prakash, L. (2004) Efficient and error-free replication past a minor-groove DNA adduct by the sequential action of human DNA polymerases ι and κ, *Mol. Cell. Biol. 24*, 5687−5693.
69. Washington, M. T., Minko, I. G., Johnson, R. E., Haracska, L., Harris, T. M., Lloyd, R. S., Prakash, S., and Prakash, L. (2004) Efficient and error-free replication past a minor-groove N^2-guanine adduct by the sequential action of yeast Rev1 and DNA polymerase ζ, *Mol. Cell. Biol. 24*, 6900−6906.
70. Minko, I. G., Washington, M. T., Kanuri, M., Prakash, L., Prakash, S., and Lloyd, R. S. (2003) Translesion synthesis past acrolein-derived DNA adduct, γ-hydroxypropanodeoxyguanosine, by yeast and human DNA polymerase η, *J. Biol. Chem. 278*, 784−790.

BI061381H